We are IntechOpen,
the world's leading publisher of
Open Access books
Built by scientists, for scientists

4,800
Open access books available

122,000
International authors and editors

135M
Downloads

Our authors are among the

154
Countries delivered to

TOP 1%
most cited scientists

12.2%
Contributors from top 500 universities

BOOK CITATION INDEX
CLARIVATE ANALYTICS
INDEXED

WEB OF SCIENCE™

Selection of our books indexed in the Book Citation Index
in Web of Science™ Core Collection (BKCI)

Interested in publishing with us?
Contact book.department@intechopen.com

Numbers displayed above are based on latest data collected.
For more information visit www.intechopen.com

Analysis and Methodology for Determining the Parasitic Capacitances in VSI-fed IM Drives Based on PWM Technique

Rudolf Ribeiro Riehl, Fernando de Souza Campos, Alceu Ferreira Alves and Ernesto Ruppert Filho

Additional information is available at the end of the chapter

Abstract

Three-phase induction motors present stray capacitances. The aim of this chapter is to present a methodology to experimentally determine these capacitances and also evaluate the effects of electromagnetic interference on motors in common mode. The proposed procedures for this methodology consist of: a) identifying the motor equivalent electrical circuit parameters through characteristic tests performed in the laboratory; b) setting up configurations between the PWM inverter and the motor for voltage and current measurements: common mode and shaft voltages, leakage and shaft (bearing) currents by using a dedicated measuring circuit; c) calculating the parasitic capacitance values between stator and frame, stator and rotor, rotor and frame and bearings of the motor using the capacitance characteristic equation; d) using the dedicated software Pspice to simulate the system composed by the three-phase induction motor fed by PWM inverter with the equivalent electrical circuit parameters; e) determining the characteristic waveforms involved in the common mode phenomenon.

Keywords: Induction motors, parasitic capacitances, PWM inverter

1. Introduction

The use of inverter controlled by pulse width modulation (PWM Inverter), on drive and control of the three-phase induction motors is increasingly common, especially for the power range of up to 10 Hp.

The recent developments in power semiconductor devices (IGBT, MOSFET, and others) have allowed these drives to achieve switching frequencies up to 20 kHz. In these frequencies, the

rise time of PWM voltage becomes very small and responsible for the appearance of phenomena, defined as electromagnetic interference (EMI) in the induction motor [12, 18, 25]. Due to the presence of parasitic capacitances in the motor caused by the free or isolated spaces between metal parts, capacitive couplings occur, which become flow paths of the high-frequency electric current between the motor phases (differential mode coupling) and between phases and the ground (common mode coupling). The higher the switching frequency, the greater are the extensions and consequences of these phenomena.

The differential mode phenomena are responsible for excessive heating of the motor, harming the electrical insulation characteristics, performance, and, consequently, their useful life, and can burn out the motor. This occurs because the PWM inverter does not feed the induction motor with a sinusoidal voltage, but by applying modulated or switched pulses, producing high-frequency harmonics, and high-voltage gradients values (high dV/dt) to the stator windings [3].

The phenomena due to the common mode are responsible for the appearance of circulating currents between motor and ground moving through the frame, bearings, and motor pedestals. As the common mode voltage is different from zero, it raises a shaft voltage between the bearing parts and the ground, which is dependent on both this common mode voltage and the parasitic capacitances that can circulate electric currents capacitive for multiple paths by the motor [10]. One of these paths passes through the bearings, and in this case the motor currents are known as bearing currents, which, due to discharges occurring at the dielectric break, can cause damages at their bearings and if the shaft locks, the motor would be forced to stop and it will cause burning of the windings. Another phenomenon that occurs is electric shock or electric discharge machining (EDM), due to the flow of leakage current motor to the frame when it is not grounded or this ground is not suitable [1, 4, 7].

The conventional method to determine these parasitic capacitances is by measuring the impedance of the induction motor using LCR Bridge [1 to 10]. In this method, the induction motor is disassembled for specific parameters to be measured. For the determination of the parameters between the stator and the motor frame, the rotor is removed and measurements are conducted with each phase bridge between the LCR and the frame and among the three phases (short-circuited in this case) and the frame. After that, the rotor is put back and its axis is short-circuited to the frame. Parameter values between stator and rotor are measured. The LCR Bridge is connected at the common point of the three phases (neutral) and the stator frame.

The parameters of the motor bearings are dynamic and depend on operating conditions (speed) of the three-phase induction motor and also the dielectric characteristics of resistivity of the lubricant temperature and the geometric construction of the motor [1 to 10]. The rotor parameters can only be determined after all previous parameters have been obtained. The LCR Bridge is connected between the rotor shaft and the frame of the induction motor.

In the absence of an LCR Bridge and an appropriate laboratory for this type of test, another methodology [40, 41] is used to determine the parameters of the equivalent circuit of the induction motor in steady state (nominal frequency) [26, 27] and for high frequency [1, 10, 14, 41], through laboratory measurements using features configurations of links between the

PWM inverter and the motor for measuring the following parameters of interest: common mode voltage (V_{CM}) and shaft voltage (V_{SHAFT}); leakage ($I_{LEAKAGE}$) and bearing (I_B) currents, by measurement circuit designed for this purpose; and calculation of the values of the parasitic capacitances between the stator and motor frame (C_{SF}), stator and rotor (C_{SR}), rotor and motor frame (C_{RF}) and bearings (C_B) using characteristic equations as will be shown in this chapter. The computer application PSPICE [36, 40] is used to simulate the three-phase induction motor powered by a PWM inverter system using the high-frequency equivalent circuit of the motor. The characteristic waveforms that represent the common mode phenomena will be obtained to allow comparisons for validation of procedures to determine the capacitance.

In this methodology [40, 41], the three-phase induction motor does not need to be disassembled and reassembled as in the case of measurement with LCR Bridge. Only the bearings are insulated, and the determination of parasitic capacitances is performed while the motor is running. The results of testing for measurement and determination of two 1 Hp induction motor parasitic capacitances and simulations, using the Pspice program, are presented.

2. Equivalent circuit of three-phase induction motor at high frequencies

At high frequencies, the capacitive reactance among the various parts of the three-phase induction motor are shown in Figure 1, which illustrates the equivalent circuit of the three-phase induction motor fed by PWM inverter [1, 6, 15]. The distributed parameters R, L, and C represent the high-frequency coupling between the windings of the stator and the rotor.

Z_{RF} is the impedance between the rotor and the motor frame, also called air gap impedance Z_g; Z_{ER} is the impedance between the windings of the stator and the rotor; Z_{SF} is the impedance between the stator windings and the frame; Z_g is the air gap impedance; and Z_B represents the impedance between the rotor and the bearing. R_W and L_W represent the equivalent impedance of the driver through which circulates the bearing current and R_g is the lead resistance connected between the frame and ground. Using the defined impedances shown by equations (1) through (4), one can obtain the high-frequency simplified circuit of the induction motor presented in Figure 2 [15]:

$$Z_{rf} = Z_g = jXC_g \tag{1}$$

$$Z_{sr} = R_{sr} + jXL_{sr} + jXC_{sr} \tag{2}$$

$$Z_{sf} = R_{sf} + jXL_{sf} + jXC_{sf} \tag{3}$$

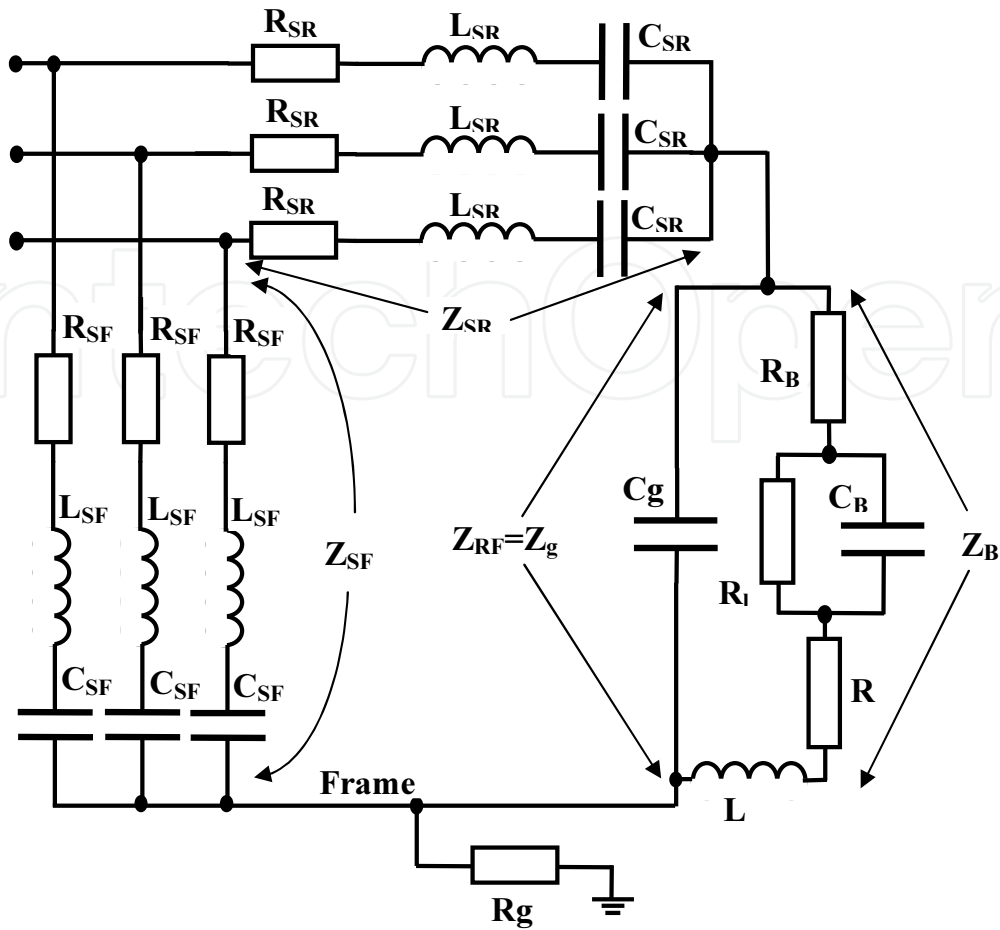$$Z_b = (R_l // jXC_b) + R_b + R_w + jXL_w \tag{4}$$

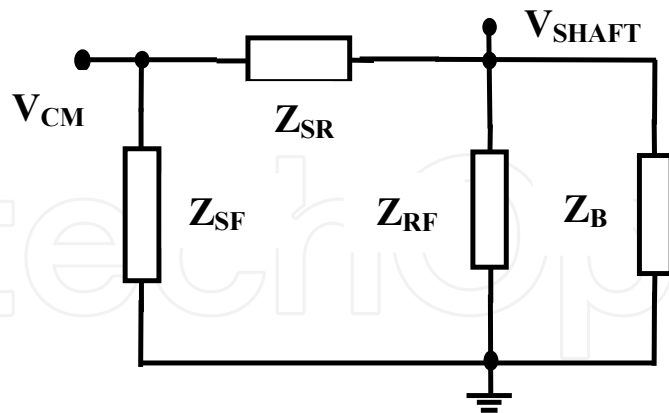**Figure 1.** High-frequency equivalent circuit of induction motor

Figure 2. High-frequency simplified circuit for three-phase induction motor according to its impedances

Simplifications of the circuit shown in Figure 2 can be done using the following considerations [1, 3, 6, 9, 10]: a) Z_{RF} is purely capacitive; b) at frequencies lower than 200 kHz, Z_{SR} assumes a capacitive characteristic; and c) Z_{SR} represents a circuit with RC behavior. At frequencies of 4–20 kHz range, which are typical switching frequencies of a PWM inverter, parasitic impedances

of the induction motor assume purely capacitive characteristic [10], according to the example shown in Figure 3.
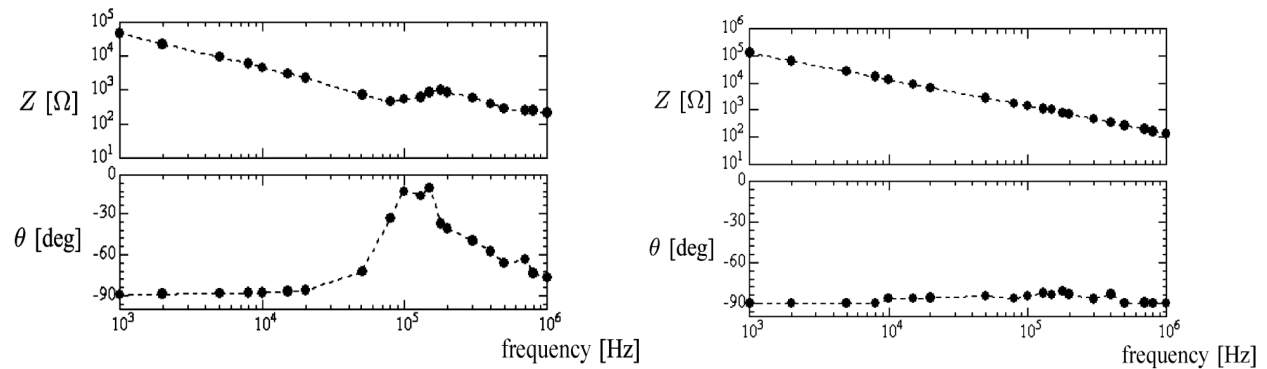

Figure 3. Capacitive impedance characteristic of the three-phase induction motor [10]

Thus, it is possible to simplify the equivalent circuit presented in Figure 2 keeping only the parasitic capacitances at the high frequencies, as shown in Figure 4.
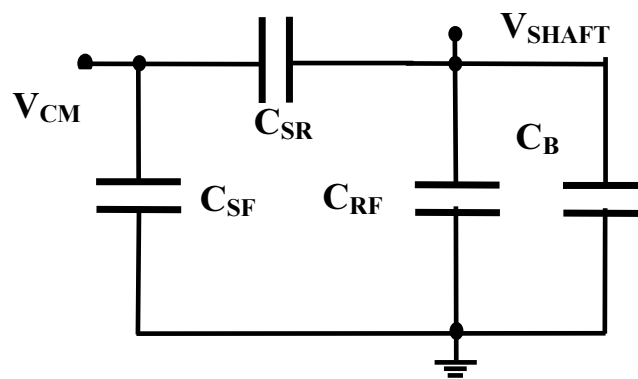

Figure 4. Simplified equivalent circuit of high-frequency induction motor

In Figure 4, V_{CM} is the common mode voltage, C_{SF} is the capacitance between the stator winding per phase and the induction motor frame, C_{SR} is the capacitance among the windings of the stator and the rotor, C_{RF} is the capacitance between the rotor and motor frame, and C_B is the capacitance of the bearing. Using this high-frequency equivalent circuit of the induction motor, the equations of both shaft voltage (V_{SHAFT}) and leakage current ($I_{LEAKAGE}$) are obtained:

$$v_{CM} = \frac{v_a + v_b + v_c}{3} \tag{5}$$

$$V_{SHAFT} = V_{CM} \cdot \left(\frac{C_{SR}}{C_{SR} + C_{RF} + C_B} \right) \tag{6}$$

$$I_{LEAKAGE} = \frac{V_{CM}}{XC_{SF}} + \frac{V_{SHAFT}}{XC_{RF}} + \frac{V_{SHAFT}}{XC_B} \tag{7}$$

The capacitances C_{SF}, C_{SR}, C_{RF}, and C_B are defined according to the geometric characteristics of both the stator as the rotor of a three-phase induction motor and its bearings [1, 2, 11, 12, 13, 23]. In [1], these capacitances are set according to the following equations, depending on the geometrical dimensions of the induction motor shown in Figure 5.

$$C_{SF} = \frac{K_{SF}.N_S.\varepsilon_r.\varepsilon_0.(W_d + W_s).L_S}{d} \tag{8}$$

$$C_{SR} = \frac{K_{SR}.N_R.\varepsilon_0.W_r.L_r}{g} \tag{9}$$

$$C_{RF} = \frac{K_{RF}.\pi.\varepsilon_0.L_r}{\ln(R_s / R_r)} \tag{10}$$

$$C_B = \frac{N_b.4.\pi.\varepsilon_0.\varepsilon_r}{(R_b + R_c / R_b - 1)} \tag{11}$$

In the above equations, K_{SF}, K_{SR}, and K_{RF} factors are stacked packages of magnetic stator and rotor, N_S and N_R are the number of slots of the stator winding and the rotor, W_s and W_d are the width and depth of the groove stator, W_r is the width of the rotor slot, L_s and L_r are the lengths of the stator and rotor slots, R_r and R_s are the radii of the stator and rotor, d is the thickness of the insulating dielectric material of the stator channel, g is the gap length, N_b is the number of bearing balls, R_b and R_c are the ball lightning and the raceway, ε_0 and ε_r are the permittivity of the medium (air and insulation). The parasitic capacitances become important when, besides the common mode voltage is different from zero, the frequency of the phase voltages becomes high, resulting in small capacitive reactance and the circuit in parallel with the remaining equivalent.

When the three-phase induction motor is fed by pure sinusoidal voltages, at the power grid frequency, the effect of these capacitances is minimal or nonexistent. If there is an unbalance in phase voltages, the common mode voltage becomes nonzero, establishing current flow through these capacitances (Figure 4) which will be significant, if the amplitudes of phase voltages are high. Thus, assuming that the motor is supplied by balanced phase voltages, the common-mode voltage (5) is zero. When the three-phase induction motor is fed through a PWM inverter, it establishes a "capacitive coupling" created by the modulated phase voltages of the inverter output. These voltages have trapezoidal characteristic value with high dV/dt of
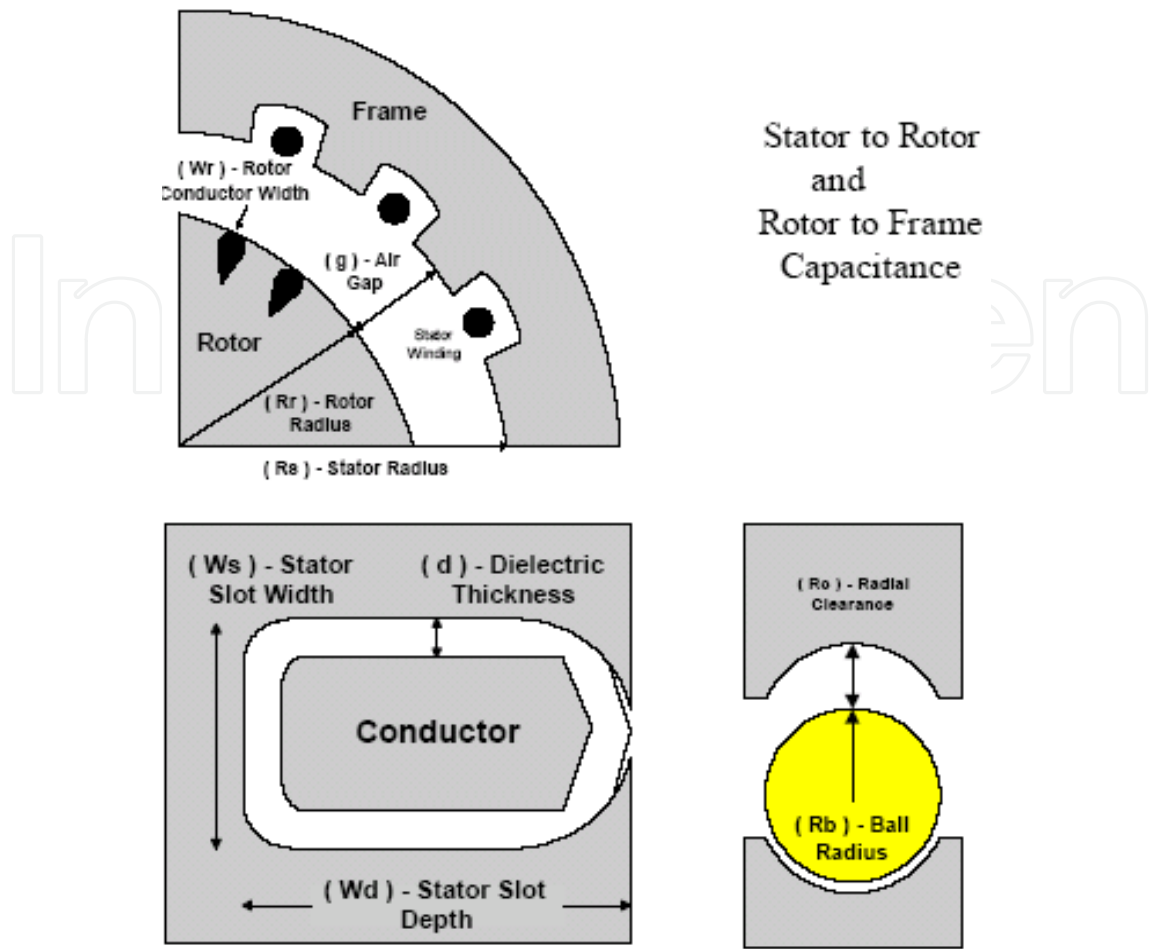
Figure 5. Dimensions – induction motor and bearing [1]

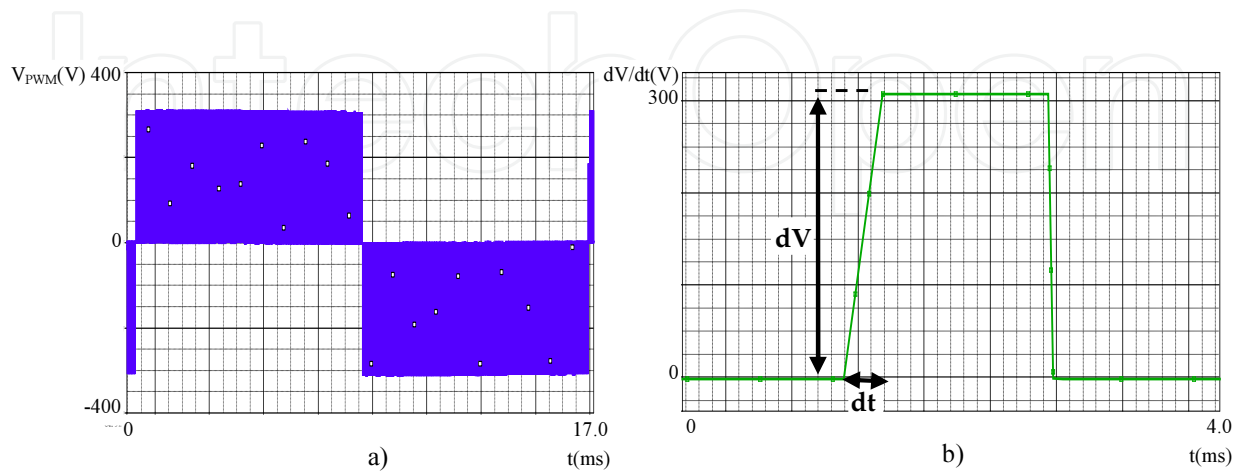the inverter while the semiconductor switches are turned on or off, as shown in Figure 6 (a, b) [12, 18, 22].

Figure 6. a) Terminal voltage of the PWM inverter, b) dV/dt voltage

As the supply voltages are not sinusoidal, the common mode voltage (V_{CM}) takes nonzero values. Thus, this voltage and also the switching frequency (f_S) of the PWM inverter now have an important role on common mode capacitive currents. For example, Figures 7a and 7b present the waveforms of the output phase voltages of the inverter and the common-mode voltage for a switching frequency (f_S) of 16 kHz.
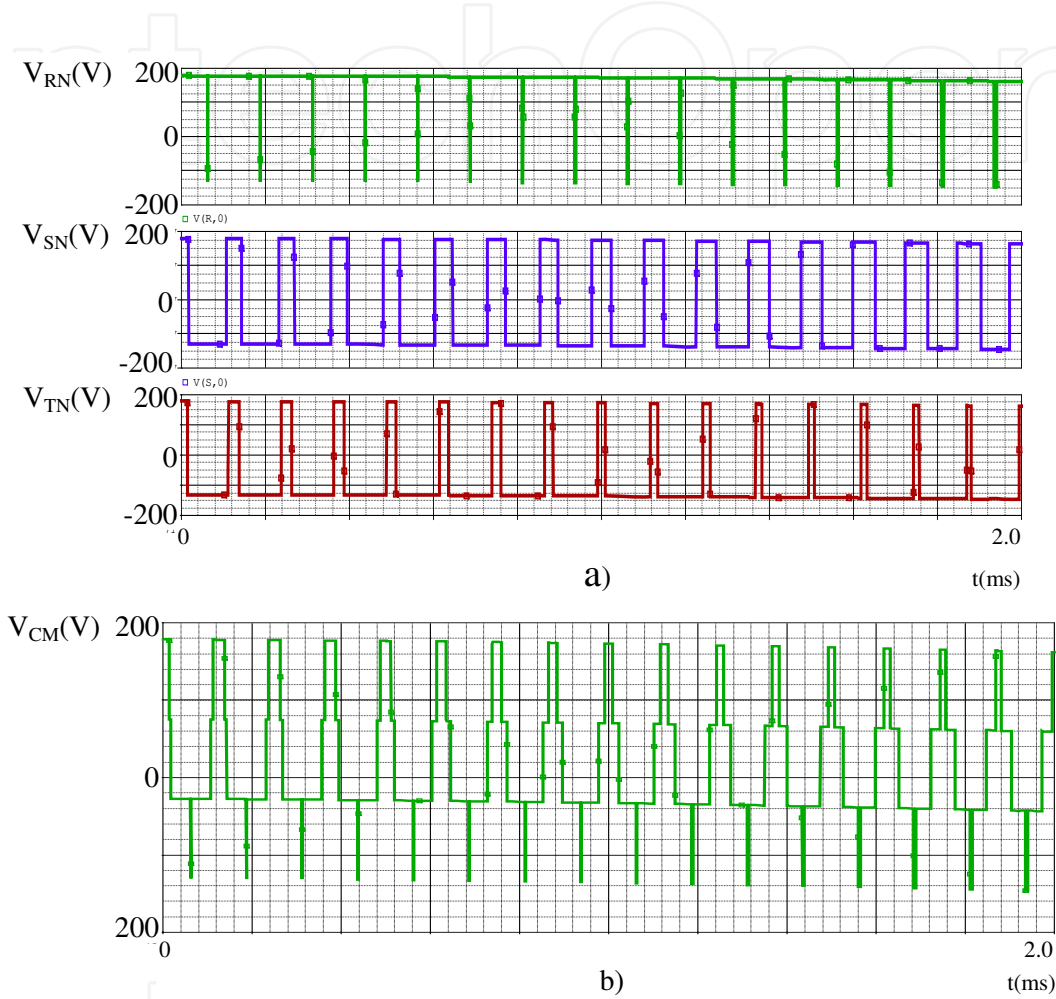
Figure 7. a) Phase voltage, b) a common mode voltage (V_{CM}) - f_S = 16 kHz

The higher the switching frequency, the better is the characteristic of the waveform of the current applied to the induction motor. Besides that, the frequency raise often implies an increase in the switching times of the IGBTs increasingly smaller, providing both increased feature dV/dt, which is directly related to the values of the capacitive currents of common mode current, as the reduction of the capacitive reactance significantly increased the amplitudes thereof. The following equations show these relationships:

$$i = C.\frac{dv}{dt} \tag{12}$$

$$I = 2.\pi.f_s.C.V \tag{13}$$

Observing equations (12) and (13), it is possible to conclude that V and I are effective values of voltage and common mode current. Thus, from the down-movement of the common-mode electrical currents (also called capacitive currents) as shown in Figure 8a [18], one can obtain the equivalent circuit of the motor for high frequency presented in Figure 8b [1 to 10].
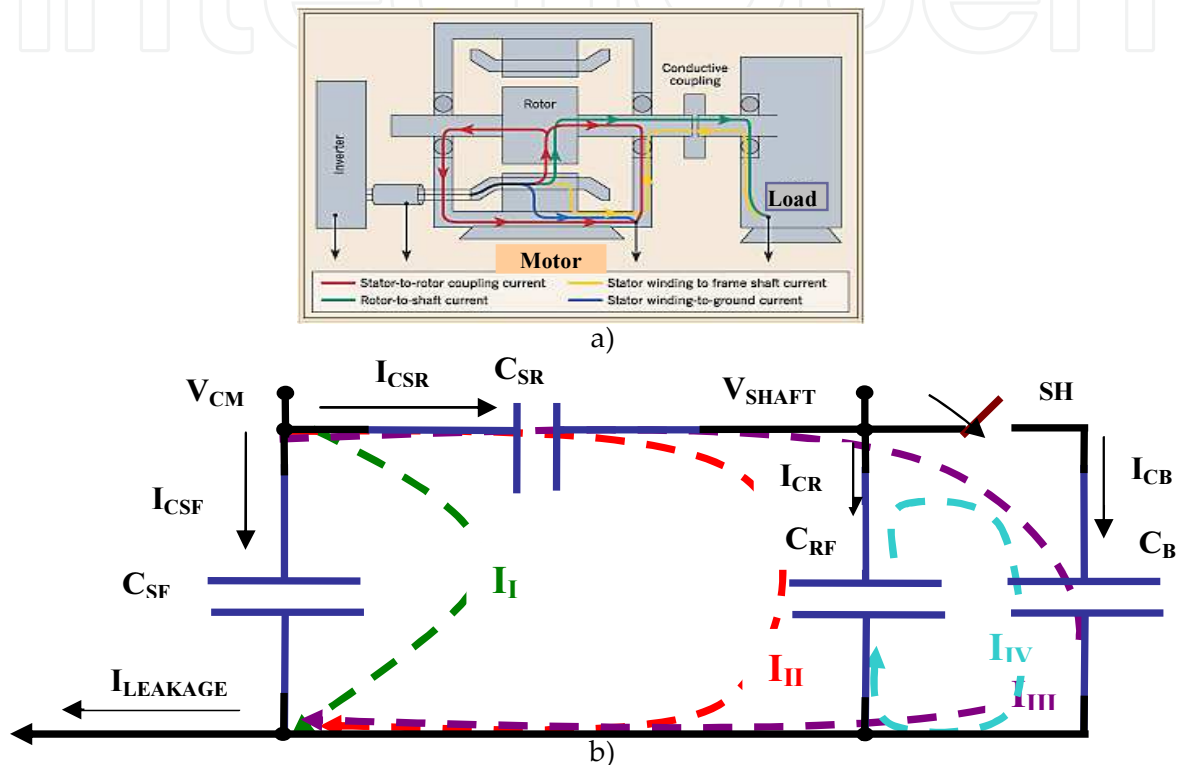

Figure 8. a) Circulating currents in the motor, b) high-frequency equivalent circuit and circulating currents [10]

The electric currents are established as follows: [10] a) II is the current flowing through the common mode voltage point (V_{CM}), which passes through the pump capacitance for the motor frame, ground or neutral and returns to the system to V_{CM} point. It is the largest component of the leakage current ($I_{LEAKAGE}$), compared to other capacitive currents because C_{SF} capacitance is much larger than others. This current is primarily responsible for the electrical discharge of the motor frame to the "ground." If the motor is not grounded to the frame satisfactorily, an important electrical discharge at various parts of it and even at the load may occur and cause an "electric shock" if someone leans on the motor frame. b) III is the current flowing through the common mode voltage point (V_{CM}), which passes through the C_{SR} and capacitances C_{RF}, motor frame, ground or neutral system and returns to the V_{CM} point. c) III is the current flowing through the common mode voltage point (V_{CM}), which passes through the C_{SR} capacitance motor shaft bearing capacitance C_B motor frame, ground or neutral system and returns to the V_{CM} point. d) IV is the current flowing shaft voltage point (V_{SHAFT}); C_{RF} capacitance thus stores

energy through the motor shaft, the switch SH, the motor frame, and returns to the C_{RF} capacitance.

The switch SH in Figure 8b is, when closed, the breaking of the bearing insulation dielectric (grease film). When this occurs, and C_{SR} is much smaller than C_{RF}, a new mesh current flow given by IV is then established. The IV mesh is responsible for the electrical discharge in the motor bearings due to the charge stored in the capacitor C_{RF}.

3. Experimental method for determination of parasitic capacitances rotor cage three-phase induction motor [40]

This item presents a methodology [40] for the determination of the parasitic capacitances of the equivalent high-frequency rotor three-phase induction motor circuit cage and the effects of electromagnetic interference caused in the same common mode, when it is driven by a PWM inverter. This is a methodology that uses an electronic circuit to measure variables needed to calculate these parameters.

The procedures proposed for the development of this methodology are: a) determination of the equivalent circuit parameters of the three-phase induction motor in steady state and high frequency and [1, 10, 15, 31] through typical laboratory test; b) establish settings of links between the PWM inverter and the motor for measurements of quantities of interest: common mode (V_{CM}) and shaft (V_{SHAFT}) voltages, leakage ($I_{LEAKAGE}$) and shaft (I_{SHAFT}) currents, developed by measuring circuit for this purpose [13, 14]; c) calculate the values of the parasitic capacitances between stator and frame (C_{SF}), stator and rotor (C_{SR}), rotor and frame (C_{RF}) and bearings (C_B), using their characteristic equations [10, 15]; d) using PSPICE [36] to simulate the system (three-phase induction motor fed by PWM inverter) with the high-frequency equivalent circuit in the same [6, 16]; e) to obtain the waveforms characteristics of the EMI phenomena.

3.1. Methodology determination procedure

The methodology determines the high-frequency equivalent circuit parameters of rotor cage three-phase induction motor, through direct measurement of quantities of interest and, using equation (14), calculate the values of the parasitic capacitances. The quantities of interest are common mode voltage (V_{CM}), shaft voltage (V_{SHAFT}), leakage current ($I_{LEAKAGE}$), and shaft current (I_{SHAFT}).

$$C = \frac{I_C}{2.\pi.f_s.V_C} \tag{14}$$

In equation (14), I_C and V_C represent the current and the effective voltage across the capacitor, respectively, and f_s the switching frequency of the PWM inverter. The schematic diagram of the methodology is shown in Figure 9.
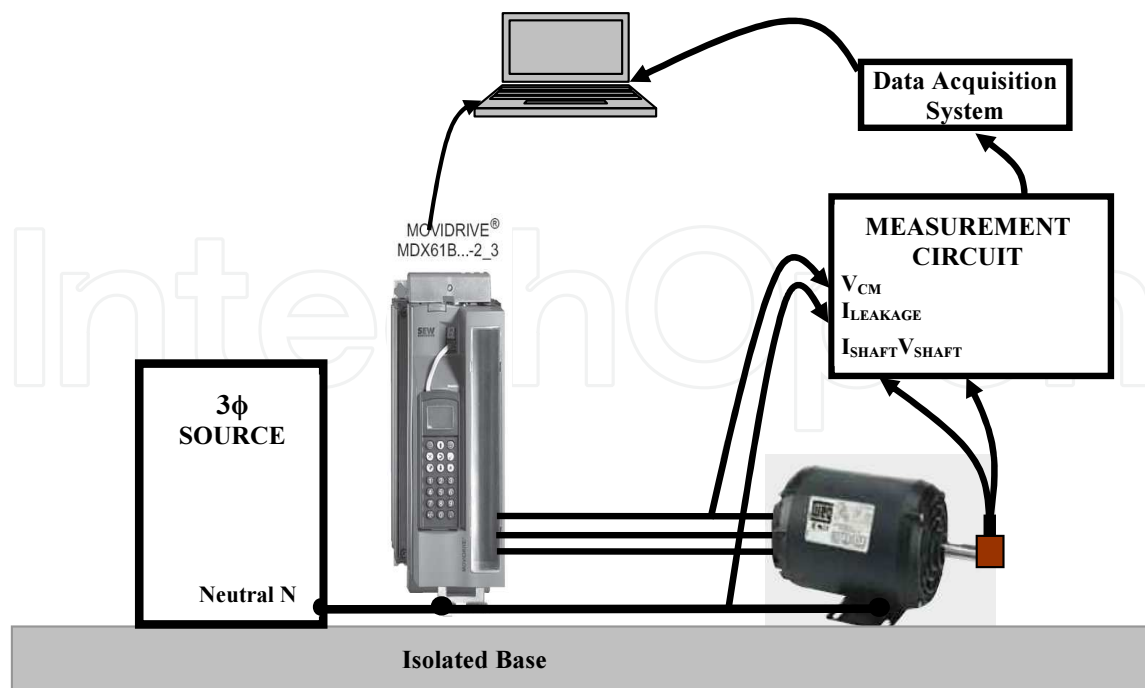
Figure 9. Schematic diagram of the methodology

The structure consists of the following equipment: three-phase power supply 220V/60Hz, 1 Hp three-phase PWM inverter, two three-phase 1Hp induction motors, measuring circuit of the quantities of interest, data acquisition board LabView, notebook PWM inverter management and signal processing through dedicated software LabView 8.5 and MOVITOOLS, base for sustaining fully insulated equipment to allow measurements, especially the currents (as close as possible to an actual situation), connecting cable with the neutral system interconnected to the PWM inverter ground terminals and the induction motor providing a circulating path to the induction motor current.

The magnitudes of the measuring circuit (V_{CM}, V_{SHAFT}, $I_{LEAKAGE,}$ and I_{SHAFT}) are shown in Figure 10. The common mode voltage (V_{CM}) is the common point of the measuring voltage (neutral) to the motor frame when it uses star connection (Y). When the same connection uses delta (Δ), it should be equivalent to a star connection using high-value resistors (1MΩ) connected to each phase of the motor with a common point (neutral). In the adjustment of the common mode voltage measurement (V_{CM}) to the acquisition board, a resistive divider (R_1, R_2, R_3, and R_4) is added so that the measured voltage does not exceed the maximum allowed by the acquisition board, that is, +/- 10V, as shown in Figure 10.

For measuring the shaft voltage (V_{SHAFT}), which is the voltage measured between the shaft and the induction motor frame, a copper ring carbon brush system is added to the induction motor shaft.

For leakage current ($I_{LEAKAGE}$) and shaft current (I_{SHAFT}) measurements, a Rogowski coil current sensor, developed for this methodology, was used [40]. The leakage current is the current measured in the connection cable between the induction motor frame and the metal frame of

the PWM inverter connected to the neutral system. It is composed of the sum of the currents flowing through the stator-frame capacitances (C_{SF}), rotor-frame (C_{RF}), and bearings (C_B).

The shaft current (I_{SHAFT}) is the current measured in the conductor which is connected to the brush and corresponding contributions from currents flowing through the rotor-frame capacitances (C_{RF}) and bearings (C_B).
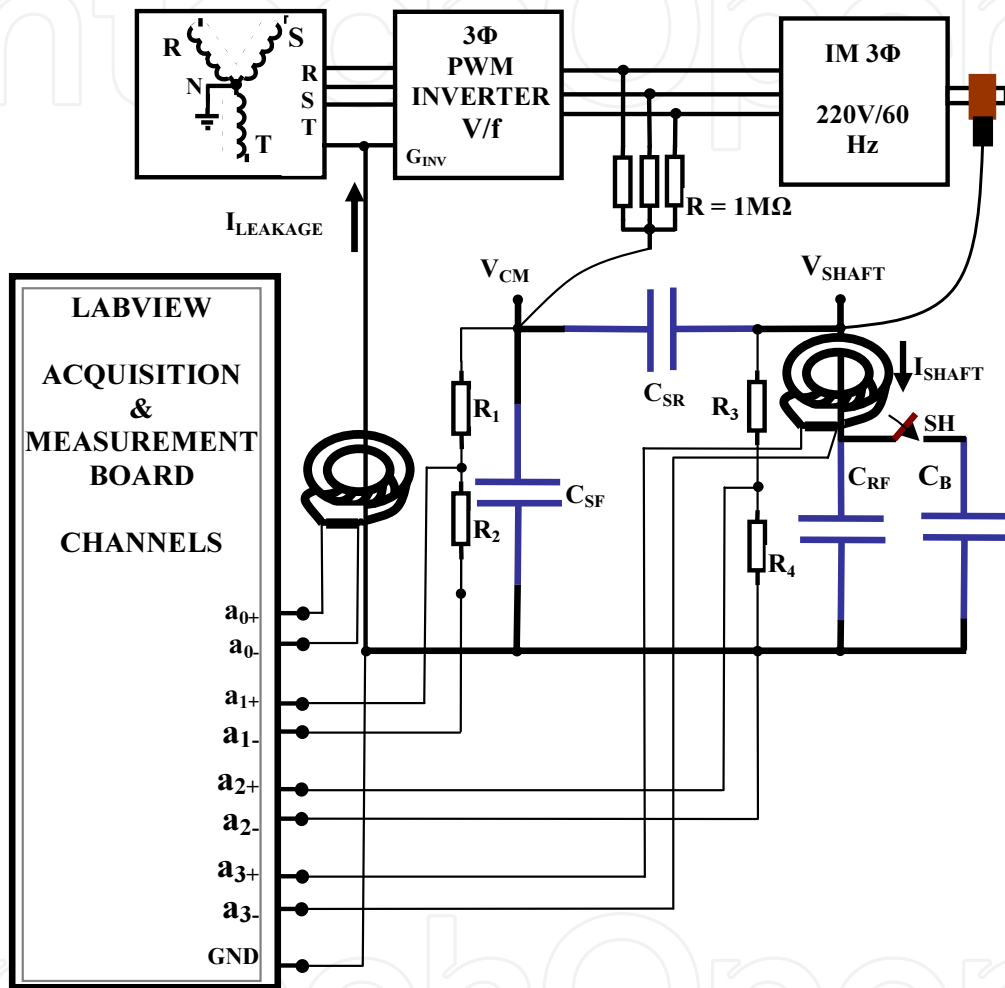

Figure 10. Measuring circuit of the quantities of interest

3.1.1. Induction motor preparation

For the application of the proposed method, the motor rotor three-phase induction cage should be prepared so that the capacitance can be determined [1, 10, 14]. Under normal conditions, the motor bearings are directly connected to both the shaft and the motor frame. It causes the capacitance existing between the rotor and the frame (C_{RF}) to short-circuit.

So the following changes are made. (a) Motor bearings are insulated by a nylon cover (tecnil) high electrical resistance. Thus, there will be no current flow by bearings (IB) and the contri-

bution branch rotor frame can be evaluated, as shown in Figure 11 [10]. (b) A conductor is connected between the external surface of one of the bearings and closest to the motor frame by a switch point. When the switch is open, there is the condition set out in item (a). When the switch is closed, then one has the rolling movement for the current frame and the returning to the bearing [10]. (c) The motor shaft settles in a ring and brush assembly, for measuring the shaft voltage (V_{SHAFT}). This system is also used to measure the shaft current (I_{SHAFT}) [14]. Figure 12 shows the items (b) and (c).
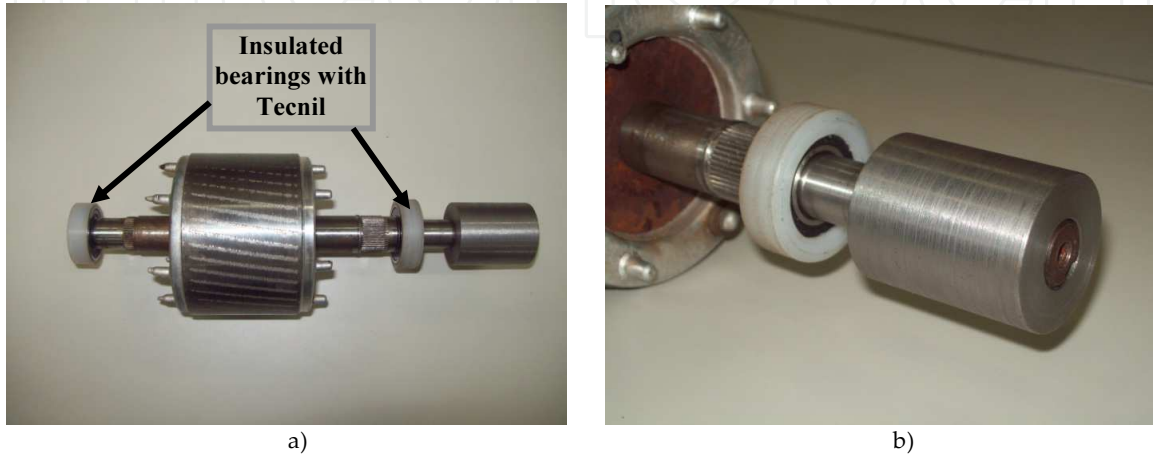

a)   b)

Figure 11. a, b): Insulation of the motor shaft bearings
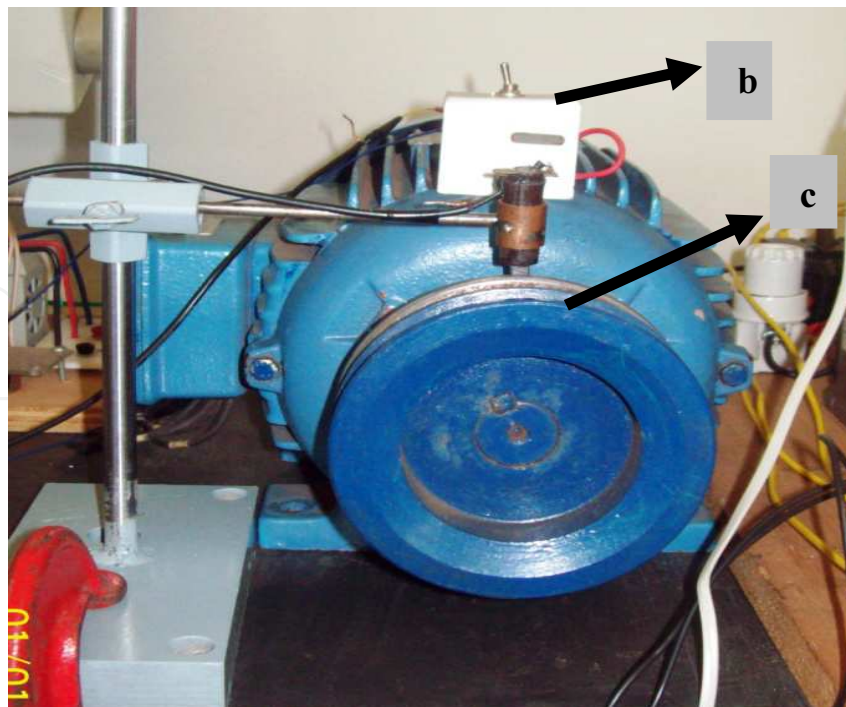

Figure 12. Switch (b) and ring-brush assembly (c) for measuring

3.1.2. Data acquisition board and measuring

In order to acquire the quantities and accomplish the measurements, LabView [32, 33, 34] platform is used. Four channels for the different measurements are defined as follows: (a) a0 channel: leakage current ($I_{LEAKAGE}$); (b) A1 channel: the common mode voltage (V_{CM}), which is set to the voltage of -10V to + 10V limits; (c) a2 channel: shaft voltage (V_{SHAFT}); and (d) a3 channel: shaft current (I_{SHAFT}).

Using dedicated software LabView 8.5, [35] created a block diagram (plant) of the measuring system for the magnitudes of interest. Figure 13 shows the block diagram for leakage current ($I_{LEAKAGE}$). The configuration for each quantity to be measured using channels with differential inputs is shown in Figure 14 to minimize the effects of common-mode voltages (noise).

Observations (Figure 13):

Block A - CORRENTE DE FUGA - Ifuga <=> LEAKAGE CURRENT - Ileakage

Block D - FILTRO RUÍDO <=> NOTCH FILTER

Block E - FILTRO PASSA-BAIXA <=> LOW-PASS FILTER

Block F - ESPECTRO - Ifuga <=> ESPECTRUM - Ileakage

Block G - RMS Ifuga_fs <=> RMS Ileakage_fs

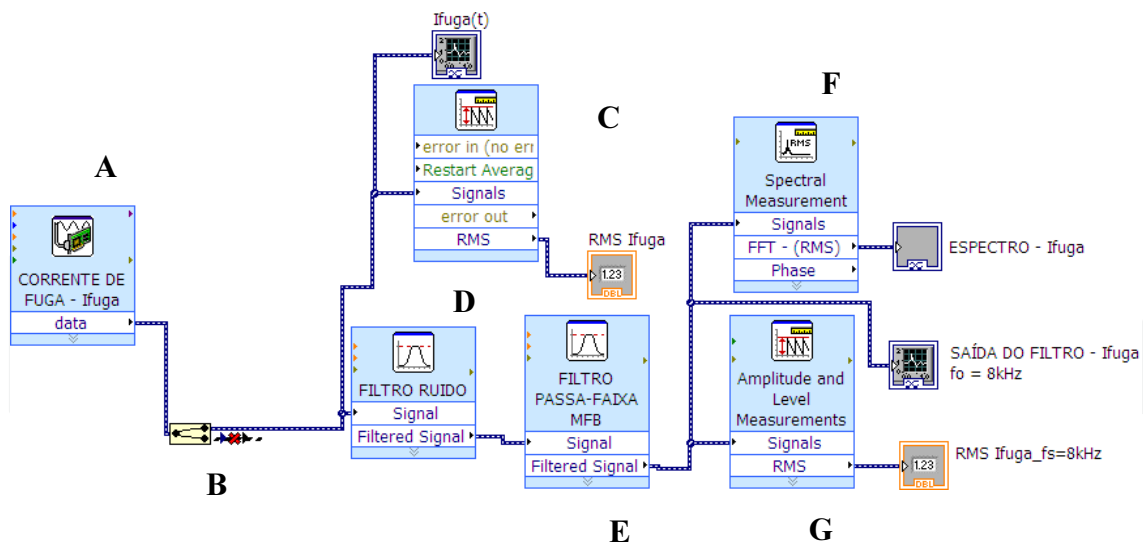SAÍDA DO FILTRO - Ifuga <=> OUTPUT FILTER – Ileakage

Figure 13. Block diagram for reading the leakage current ($I_{LEAKAGE}$)

Using the DAQ block (A), the following items are defined for each channel: a) type of quantity (voltage or current), b) name of greatness and sample rate, c) type of sampling, d) connection diagram channel and other settings which depend on the desired type of measurement. Can be used up to 16 signals for reading.
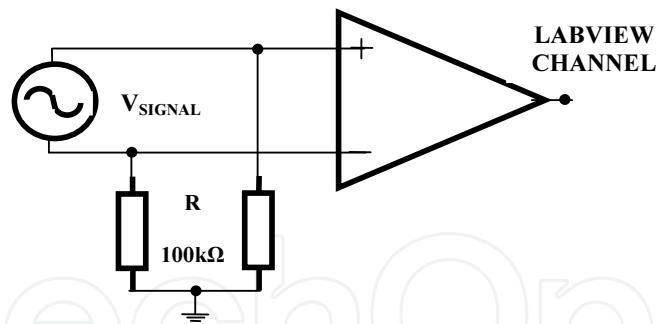
Figure 14. Differential input of the A/D channels

Signals Using Split (B) block quantities of simultaneous readings can be made. In this case, there are 4 outputs. The current $I_{LEAKAGE}$ a function of time is shown on the oscilloscope $I_{LEAKAGE}$ (t).

The Amplitude and Level Measurements block (C) allows for the signs readings DC values (DC) and effective (RMS). The value is shown on the display "RMS $I_{LEAKAGE}$."

The blocks Noise Filter (D) and Pass Filter Range MFB (E) treat the signal so that it can be measured on the switching frequency of the PWM inverter. The filtered signal is displayed on the oscilloscope FILTER OUT – $I_{LEAKAGE}$.

Noise Filter (NOTCH) has the function of not allowing passage of signals of a frequency band or a specific frequency. The Band Pass Filter MFB allows only the frequency band specified signal to pass. This filtering block allows you to define: a) type of filter: low-pass, high-pass, band-pass, band-reject; b) frequency band; c) the type of response: finite impulse response (FIR) or infinite impulse response (IIR); d) topology: Butterworth, Chebyshev, Inverse Chebyshev, Elliptic, and Bessel.

Spectral Measurement block (F) shows the oscilloscope through the spectrum $I_{LEAKAGE}$ already filtered at the desired frequency. And the block (G) similar to block (C) provides effective current at switching frequency f_S, available in display RMS_$I_{LEAKAGE}$_f_S. This entire procedure aims to ensure that measurements are made in order to respect the equation for calculating the capacitance (14).

3.1.3. PWM inverter

The PWM inverter used in this study is a new generation of static power converters that feature improvements in its modular structure, providing better functions in the lower-frequency range and greater overload capacity. Introducing control functions integrated with the possibility of use of communication accessories, this enables applications to AC inverter drive systems requiring high efficiency in a power range 0.55–160 kW.

The Inverter MOVIDRIVE MDX60B/61B [29] has the following main characteristics: a) The MOVIDRIVE MDX61B model allows application for asynchronous motors (induction motor) with or without encoder feedback, synchronous and asynchronous servomotors. b) Control modes: VFC (Voltage Flux Control): to control induction motors. Using encoder feedback, it

operates with vector control activated. If there is no feedback loop, it operates with V/f control (scalar) and CFC (Current Flux Control); for controlling synchronous and asynchronous servomotors it always operates with encoder feedback. The inverter model used in this work is the Movidrive MDX61B 0037-2A3-4-0 with the following characteristics: Power 5 Hp (3.7 kw); phase power supply: 220 V/50–60 Hz; rated output current: 15.2 A and PWM switching frequency: 4, 8, 12, and 16 kHz. Using MOVITOOLS [31] dedicated program, both the switching frequency f_S of the inverter induction motor as well as the rotational speed can be changed, allowing a more complete analysis of the behavior of the parasitic capacitances to be realized.

3.2. Tests laboratory procedure

A procedure was adopted within the Electrical Machines Laboratory for the measurement tests so that determining the high-frequency capacitance of the induction motors could be carried out in conditions where there is the least possible interference in the results thereof. These procedures are described as follows: a) Ensure the total isolation of the set: three-phase induction motor being tested and PWM inverter from the base where they are supported in order that there is no current flow to the system from the motor frame and the inverter. b) Verification of the connections between the motor frame and the inverter with the NEUTRAL of three-phase power supply, allowing you to create a single movement path of the motor leakage current and hence its correct measurement. c) The entire measurement system (LABVIEW acquisition board) and the computer (notebook) used in the execution of dedicated programs and measured data storage must be the same reference system NEUTRAL. This ensures reliable measurements. d) Correct positioning and enough brush pressure in the ring, the induction motor shaft, ensuring good contact and, therefore, reliable measurements of shaft voltage and current (V_{SHAFT} and I_{SHAFT}). e) Check all connections of the acquisition system/measurement and inverter with the computer. f) carrying out the tests in air-conditioned environment, to ensure the same conditions for the other tests, and g) if possible, work with a fully isolated power system, not only using an isolating transformer, but also ensuring electrical insulation. This way, voltage and current of the supply system will always be the same in any situation and time, providing measurements and better results. Following these procedures, tests of induction motors to determine the parasitic capacitances can be started.

3.3. Parasitic capacitances determination of the rotor cage three-phase induction motor

The high-frequency equivalent circuit is shown again in Figure 15.

When determining the capacitance the following procedure should be followed: a) Switch SH open: Motor bearings are isolated. So there is no current flowing through the bearings and the C_B capacitance does not contribute to the value of B_{VR} (Bearing Voltage Ratio). b) Switch SH closed: a circulating current starts to flow through the bearings, and the C_B capacitance becomes to influence the value of B_{VR}.

Measurements are performed in the following quantities of interest: common mode voltage (V_{CM}), shaft voltage (V_{SHAFT}), leakage current ($I_{LEAKAGE}$) shaft current with SH off (I_{SHAFT}-OFF),
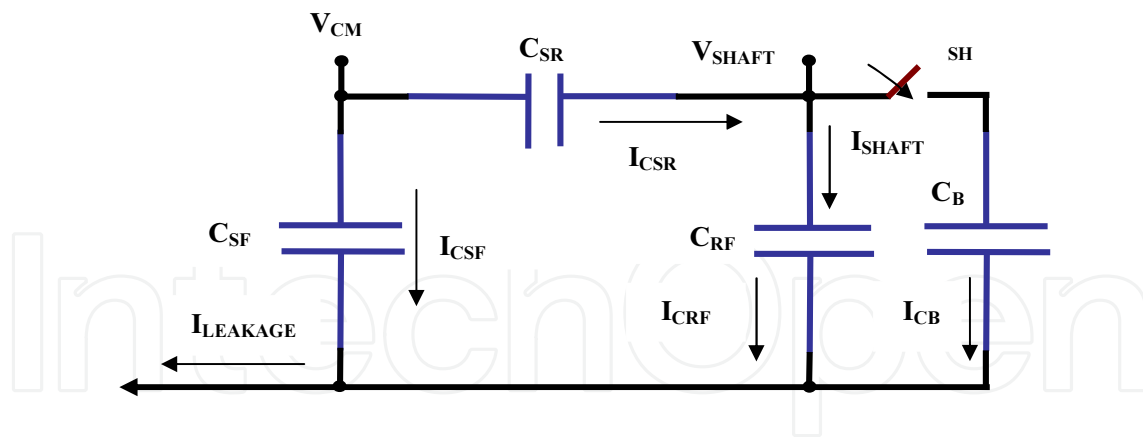
Figure 15. Simplified equivalent circuit of high-frequency induction motor

shaft current with SH on ($I_{SHAFT-ON}$). The following values are determined from the following streams:

$$I_{C_{SF}} = I_{LEAKAGE} - I_{SHAFT-OFF} \tag{15}$$

$$I_{C_{SR}} = I_{C_{RF}} = I_{SHAFT-OFF} \tag{16}$$

$$I_{C_B} = I_{SHAFT-OFF} - I_{SHAFT-ON} \tag{17}$$

The parasitic capacitances of the induction motor: C_{SF}, C_{RF}, C_{SR}, and C_B are determined through the rewritten equations below:

$$C_{SF} = \frac{I_{C_{SF}}}{2.\pi.f_s.V_{CM}} \tag{18}$$

$$C_{RF} = \frac{I_{C_{RF}}}{2.\pi.f_s.V_{SHAFT}} \tag{19}$$

$$C_{SR} = \frac{I_{C_{SR}}}{2.\pi.f_s.\left(V_{CM} - V_{SHAFT}\right)} \tag{20}$$

$$C_B = \frac{I_{C_B}}{I_{C_{RC}}} \cdot C_{RC} \tag{21}$$

4. Measurements and simulations

The method described in the previous section was applied in three-phase induction motors (two 1 Hp motors). One of the 1 Hp motors no longer presents its original features because the stator windings were fully replaced without regard to the original design features. This procedure allowed to check if there were changes (or not) in the values of the capacitances for the other 1 Hp motor, which presents original project features, since the objective is to ratify that the parasitic capacitances depending only on geometric-constructive features of the motor. Since the determination of the capacitances depends on the quantities of interest at high frequency, the tests may be performed with or without load on the shaft of the induction motors.

4.1. Test of three-phase induction motors

4.1.1. Determination of low-frequency parameters

Initially, tests for determining the low-frequency equivalent circuit (nominal) parameters of the motors were performed [27, 37]. The parameters were determined from characteristic tests using the two wattmeter method: test empty and locked rotor test with characteristic equations [26, 27]. The equivalent circuit parameters of the two induction motors 1 Hp shown in Table 1 were determined. These parameters are used in the simulation using PSPICE for analysis and comparison with the results obtained in the laboratory (Figure 16).

The two three-phase induction motors used in this test are as follows: a) manufacturer: WEG, b) rated power: 1 Hp, c) nominal voltage: 220V (Δ) / 380V (Y) d) current nominal: 3,8A (Δ) and 2,4a (Y), e) rated speed: 1710 rpm, f) number of poles: 4.

Motor (Hp)	$R_1(\Omega)$	$R_2{}'(\Omega)$	$L_1= L_2$ (mH)	L_{mag}(mH)
1 (IM1hp1)	8.55	5.62	16.95	346.31
1 (IM1hp2)	8.70	6.53	18.22	366.40

Table 1. The low-frequency equivalent circuit parameters determined from laboratory
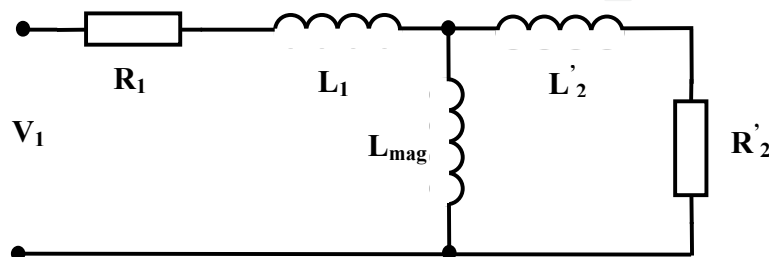

Figure 16. Equivalent circuit of low-frequency induction motor

4.1.2. High-frequency parameters determination

Using the application program MOVITOOLS [31], the PWM inverter is parameterized in terms of induction motor characteristics to be tested (plate data) as well as the drive and operating characteristics. PWM switching frequency and fundamental frequency of the induction motor can be changed in real time.

The application program LabView [35] was set to adjust the frequencies of noise filters and band pass of the quantities of interest to the switching frequency of the PWM inverter.

After all measurements and calculations, the parasitic capacitance curves were constructed: a) capacitance as a function of motor drive frequency (Hz) to a fixed switching frequency, b) capacitance as a function of the switching frequency to drive 60 Hz motor, c) mean value of capacitance as a function of the switching frequency. The waveforms of the quantities of interest were also obtained by measuring with a digital oscilloscope.

4.2. Test of three-phase induction motors of 1 Hp

4.2.1. Motor IM1hp1

The three-phase induction motor 1 Hp (IM1hp1) is connected to stator winding delta (Δ), and 220 V line voltage. A star configuration equivalent to the common mode voltage measurement (V_{CM}) is well utilized. Table 2 shows the measured values of the quantities of interest. Table 3 shows the calculated values of the currents flowing between the stator and the motor frame (I_{CSF}) and bearings (I_{CB}). Table 4 shows the calculated values of the three-phase induction motor parasitic capacitances 1Hp IM1hp1.

Measurements and calculations of quantities of interest of parasitic capacitances of the two induction motors were made to switching frequencies of 12 and 16 kHz. The results for the switching frequencies of 4 and 8 kHz can be observed in [40].

Inverter Switching Frequency (kHz)	Motor Frequency (Hz)	V_{CM} (V)	V_{SHAFT} (V)	$I_{LEAKAGE}$ (mA)	$I_{SHAFT-OFF}$ (mA)	$I_{SHAFT-ON}$ (mA)
12						
	20	93,31	4,36	14,30	0,456	0,382
	30	82,17	3,87	12,45	0,393	0,344
	40	67,42	3,18	10,53	0,343	0,303
	50	50,57	2,37	7,83	0,247	0,218
	60	33,11	1,57	5,23	0,169	0,153
16						
	20	93,91	4,51	19,40	0,544	0,440
	30	83,98	4,08	17,30	0,490	0,412
	40	69,23	3,37	14,20	0,403	0,341

Inverter Switching Frequency (kHz)	Motor Frequency (Hz)	V_{CM} (V)	V_{SHAFT} (V)	$I_{LEAKAGE}$ (mA)	$I_{SHAFT-OFF}$ (mA)	$I_{SHAFT-ON}$ (mA)
	50	51,77	2,53	10,50	0,302	0,257
	60	33,71	1,67	7,03	0,202	0,175

Table 2. Measurement of quantities of interest of 1Hp motor IM1hp1

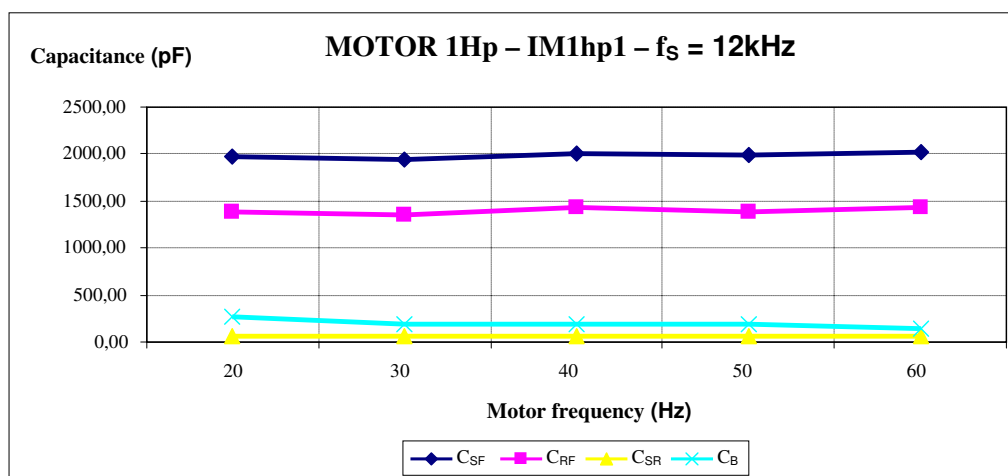| Inverter Switching Frequency (kHz)	Motor Frequency (Hz)	Ic_{SF} (mA)	Ic_{B} (mA)
12			
	20	13,84	0,07
	30	12,06	0,05
	40	10,19	0,04
	50	7,58	0,03
	60	13,84	0,07
16			
	20	18,86	0,10
	30	16,81	0,08
	40	13,80	0,06
	50	10,20	0,05
	60	6,83	0,03

Table 3. Calculated currents – IM1hp1

Inverter Switching Frequency (kHz)	Motor Frequency (Hz)	C_{SF} (pF)	C_{RF} (pF)	C_{SR} (pF)	C_{B} (pF)
12					
	20	1967,82	1387,17	67,99	268,72
	30	1946,16	1346,89	66,57	191,85
	40	2004,05	1430,60	70,82	188,86
	50	1988,84	1382,29	67,97	183,88
	60	2027,35	1427,71	71,07	149,30
16					
	20	1997,33	1199,87	60,53	283,61
	30	1991,15	1194,67	61,00	226,18

Inverter Switching Frequency (kHz)	Motor Frequency (Hz)	C_{SF} (pF)	C_{RF} (pF)	C_{SR} (pF)	C_B (pF)
	40	1982,45	1189,56	60,87	216,28
	50	1959,52	1187,41	61,01	207,91
	60	2014,87	1203,23	62,72	185,64

Table 4. Parasitic capacitances motor 1Hp IM1hp1

Figure 17 shows the values of each of the parasitic capacitances on the basis of the motor frequency (speed) specific to the switching frequency of the PWM inverter 12 kHz and 16 kHz.

a)
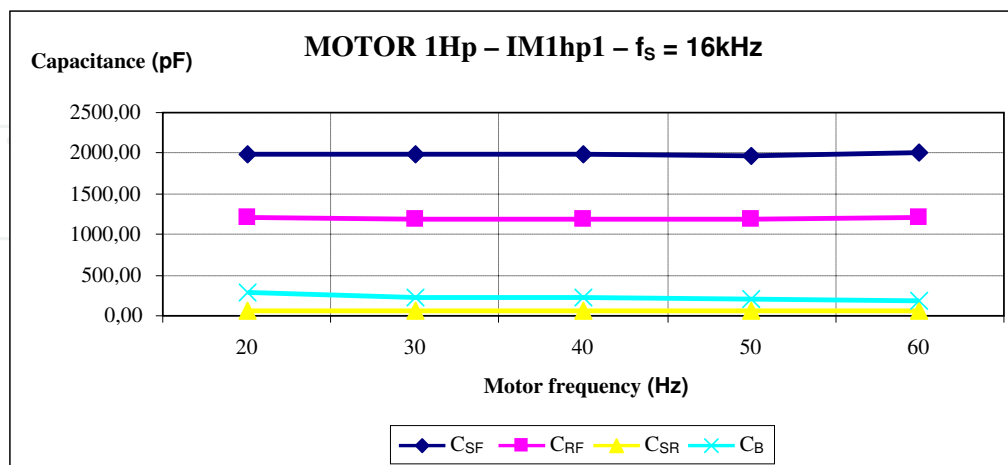
b)

Figure 17. Parasitic capacitances due to motor frequency of 1 Hp (IM1hp1) for 12 kHz (a) and 16 kHz (b) inverter switching frequency

The capacitances C_{SF}, C_{RF}, C_{SR} are almost constant for the variation of the motor frequency and the switching frequency of the PWM inverter, indicating that they depend mainly on the geometric characteristics of the motor [1].

In turn, the C_B capacitance decreases with increasing motor frequency (increase the speed). This is because, besides being dependent on the dimensions of the bearing, this capacitance is also a function of speed [10].

Figure 18 shows the values of the parasitic capacitances on the basis of the switching frequency of the PWM inverter to the motor frequency of 60Hz. The results confirm that the parasitic capacitances depend exclusively on the physical constructive characteristics of the induction motor.
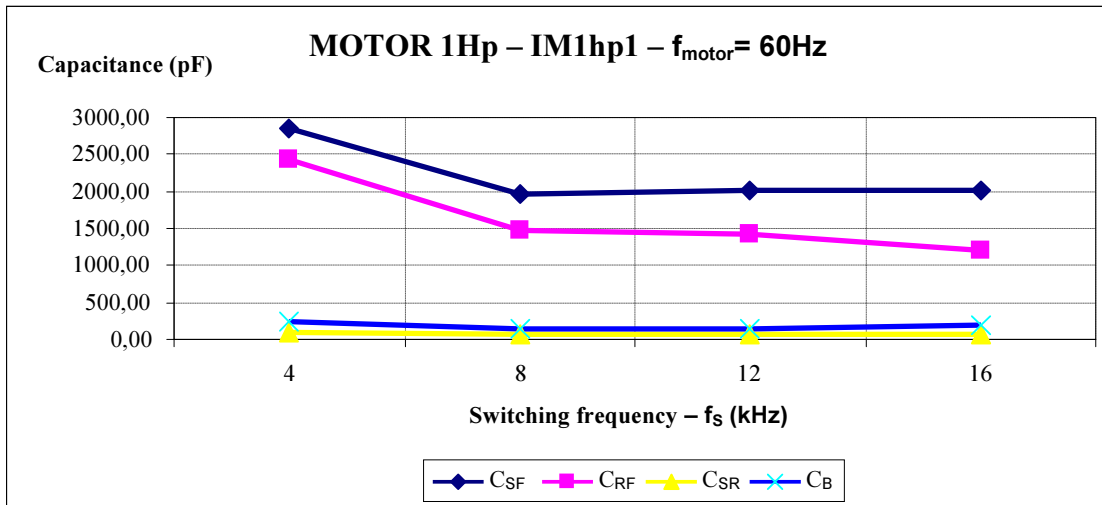

Figure 18. Capacitances due to the motor switching frequency of 1 Hp (IM1hp1) power frequency 60 Hz

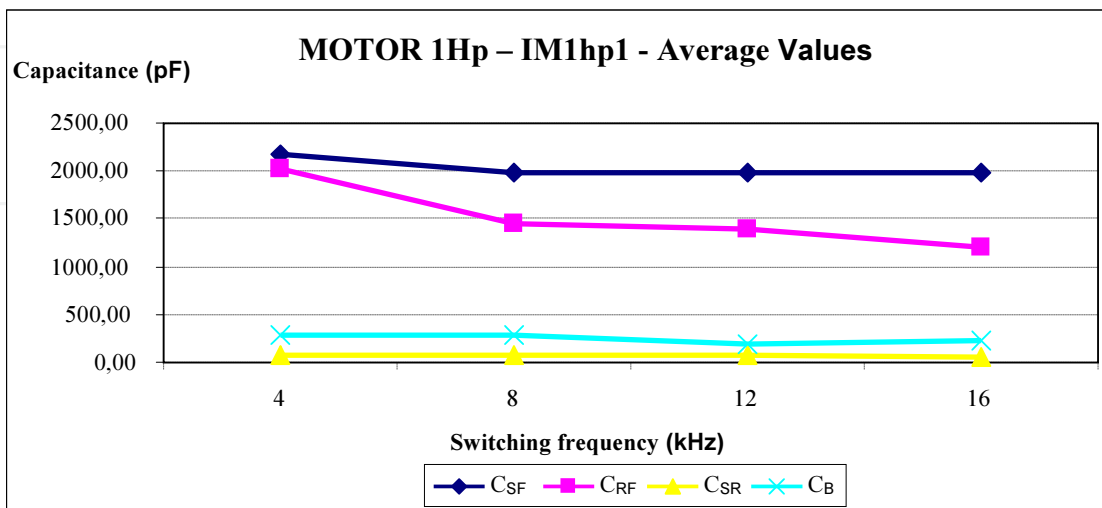Figure 19 presents the average parasitic capacitance values of the motor 1 Hp IM1hp1.

Figure 19. Average values of the capacitances for 1 Hp motor (IM1hp1)

4.2.2. Motor IM1hp2

The results for the second three-phase induction motor 1Hp, IM1hp2 are shown below. Table 5 presents the measured values of the quantities of interest.

Table 6 presents the calculated values of the currents flowing between the stator and the motor frame (I_{CSF}) and bearings (I_{CB}).

Table 7 presents the calculated values of the three-phase induction motor parasitic capacitances of 1 Hp IM1hp2.

Inverter Switching Frequency (kHz)	Motor Frequency (Hz)	V_{CM} (V)	V_{SHAFT} (V)	$I_{LEAKAGE}$ (mA)	$I_{SHAFT-OFF}$ (mA)	$I_{SHAFT-ON}$ (mA)
12						
	20	95,42	4,20	14,84	0,393	0,211
	30	85,58	3,74	13,10	0,343	0,222
	40	70,13	3,18	10,93	0,284	0,207
	50	52,68	2,37	8,15	0,222	0,185
	60	34,62	1,53	5,45	0,149	0,133
16						
	20	95,12	4,35	20,00	0,530	0,327
	30	84,88	3,97	18,46	0,478	0,326
	40	69,83	3,31	15,18	0,404	0,313
	50	52,98	2,48	11,10	0,303	0,261
	60	34,31	1,65	7,67	0,212	0,187

Table 5. Measurement of quantities of interest – IM1hp2

Inverter Switching Frequency (kHz)	Motor Frequency (Hz)	Ic_{SF} (mA)	Ic_B (mA)
12			
	20	14,45	0,18
	30	12,76	0,12
	40	10,65	0,08
	50	7,93	0,04

Inverter Switching Frequency (kHz)	Motor Frequency (Hz)	Ic_{SF} (mA)	Ic_{B} (mA)
	60	5,31	0,02
16			
	20	19,47	0,20
	30	17,98	0,15
	40	14,78	0,09
	50	10,80	0,04
	60	7,46	0,03

Table 6. Calculated currents – IM1hp2

Inverter Switching Frequency (kHz)	Motor Frequency (Hz)	C_{SF} (pF)	C_{RF} (pF)	C_{SR} (pF)	C_{B} (pF)
12					
	20	2008,24	1239,80	57,09	1062,69
	30	1977,10	1215,68	55,55	661,51
	40	2013,30	1185,36	56,30	442,07
	50	1995,63	1244,62	58,64	253,24
	60	2032,70	1291,66	59,73	159,75
16					
	20	2036,24	1212,65	58,06	749,66
	30	2107,39	1196,70	58,72	554,36
	40	2104,88	1212,93	60,35	349,10
	50	2027,39	1215,36	59,69	196,66
	60	2163,08	1280,51	64,68	172,38

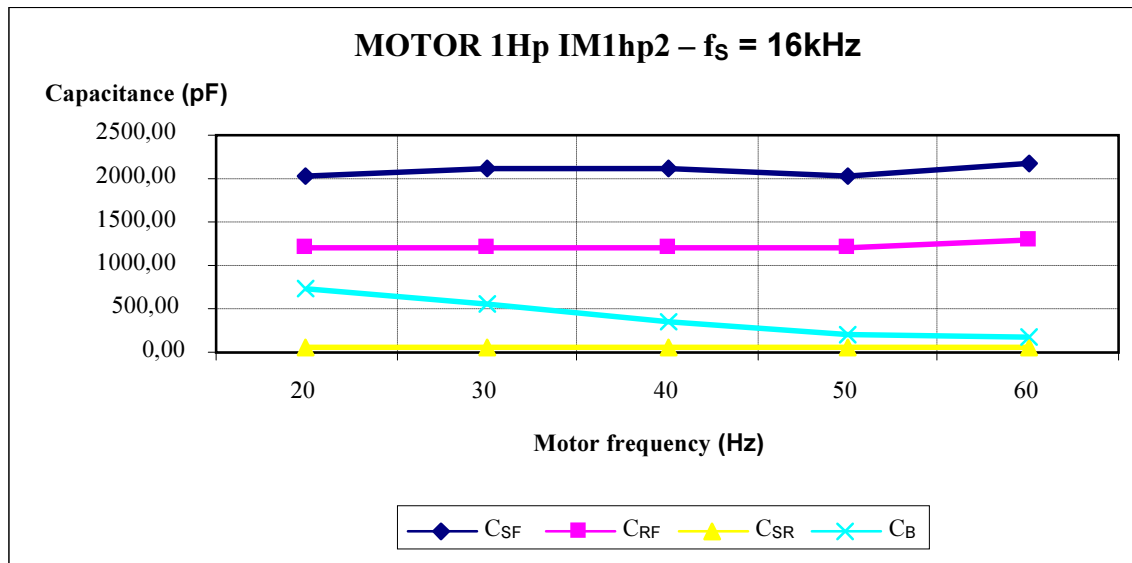**Table 7.** Parasitic capacitances of motor 1 Hp IM1hp2

Figure 20 shows the values obtained for the parasitic capacitance depending on the motor frequency, for specific switching frequency of the PWM inverter 12 kHz and 16 kHz.

The same behaviors found in the motor 1Hp IM1hp1 were observed.

Figure 21 shows the values of the parasitic capacitances on the basis of the switching frequency of the PWM inverter to the motor frequency of 60Hz.
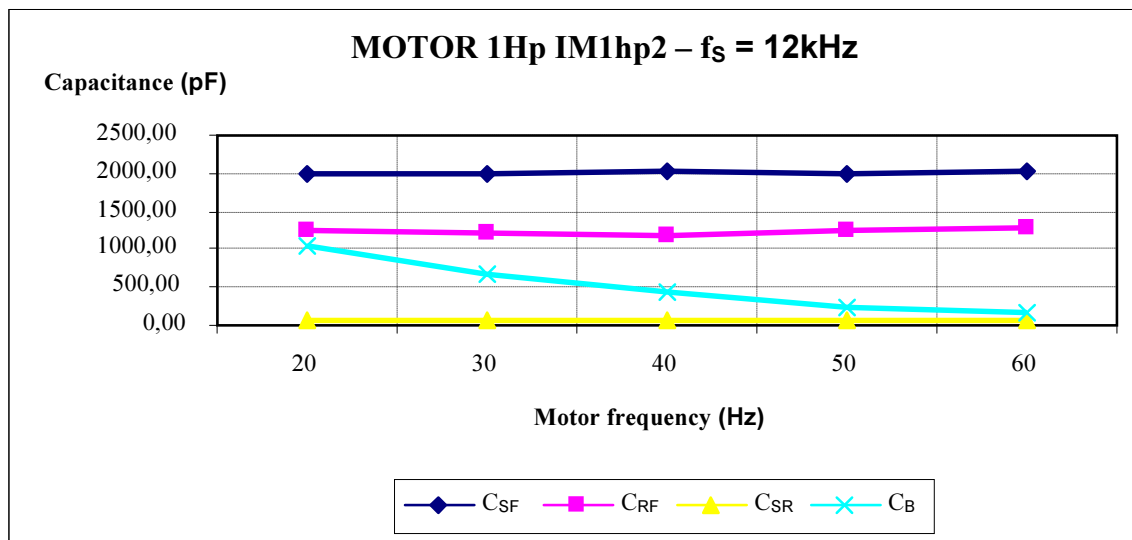
a)

b)

Figure 20. a),b) Parasitic capacitances due to motor frequency for different inverter switching frequency (IM1hp2)

Figure 22 presents the average values of parasitic capacitance of motor 1 Hp IM1hp2.

4.3. Simulations and measurements

The software Pspice [30, 36] was used to simulate the methodology and compare the wave-forms obtained in the simulations with actual measurements made using digital oscilloscope. The schematic circuit simulation is shown in Figure 23.

The schematic circuit comprises: a) inverter structure with three-phase supply, three-phase rectifier without control (diodes) with DC bus, and three-phase inverter bridge; b) equivalent
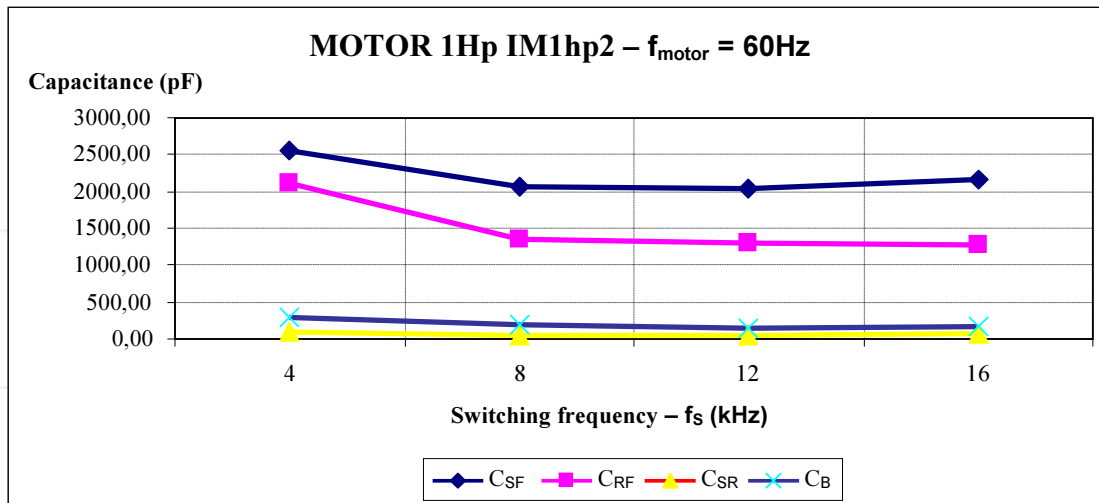
Figure 21. Capacitances due to the motor switching frequency of 1 Hp (IM1hp2) motor frequency 60 Hz
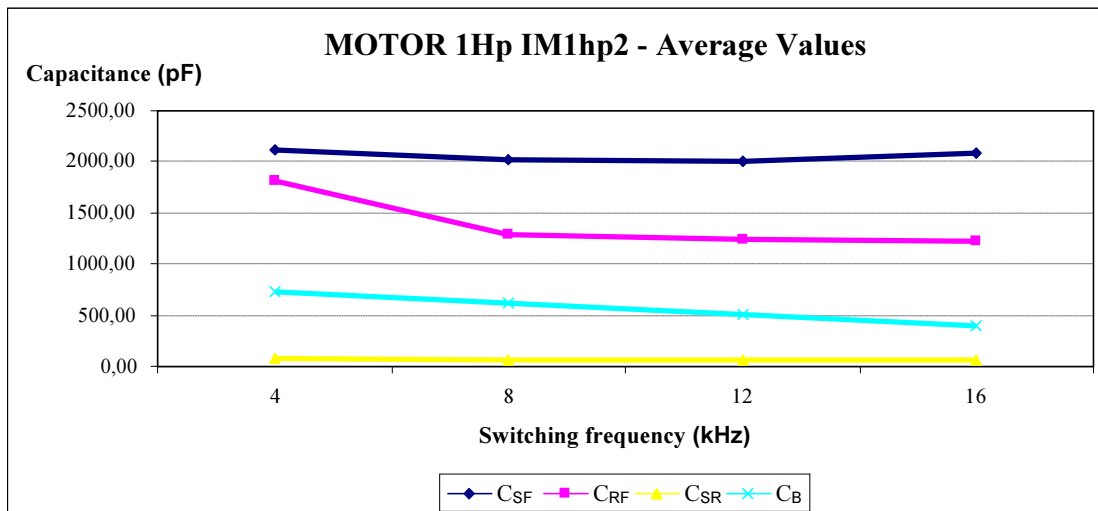

Figure 22. Average values of capacitance for the motor 1 Hp IM1hp2

circuit of low-frequency induction motor; c) equivalent circuit of high-frequency three-phase induction motor; and d) signal generator with pulse width modulation (PWM).

The charts below show waveforms that appear in the named graphs (a) are results of measurements by using digital oscilloscope. The forms of common mode voltage wave (V_{CM}) are attenuated to match the oscilloscope's full-scale capacity. The waveforms that appear in the named graphs (b) are obtained by using PSPICE simulation application. Without loss of generality, in the simulation (Figure 23) are used ideal components of semiconductor switches that facilitate the process of solving differential equations reducing convergence problems.

The waveforms shown below are the quantities of interest with switching frequency of 16 kHz PWM inverter and frequency of 60 Hz motor to three-phase induction motors of 1 Hp (IM1hp1 and IM1hp2), respectively.
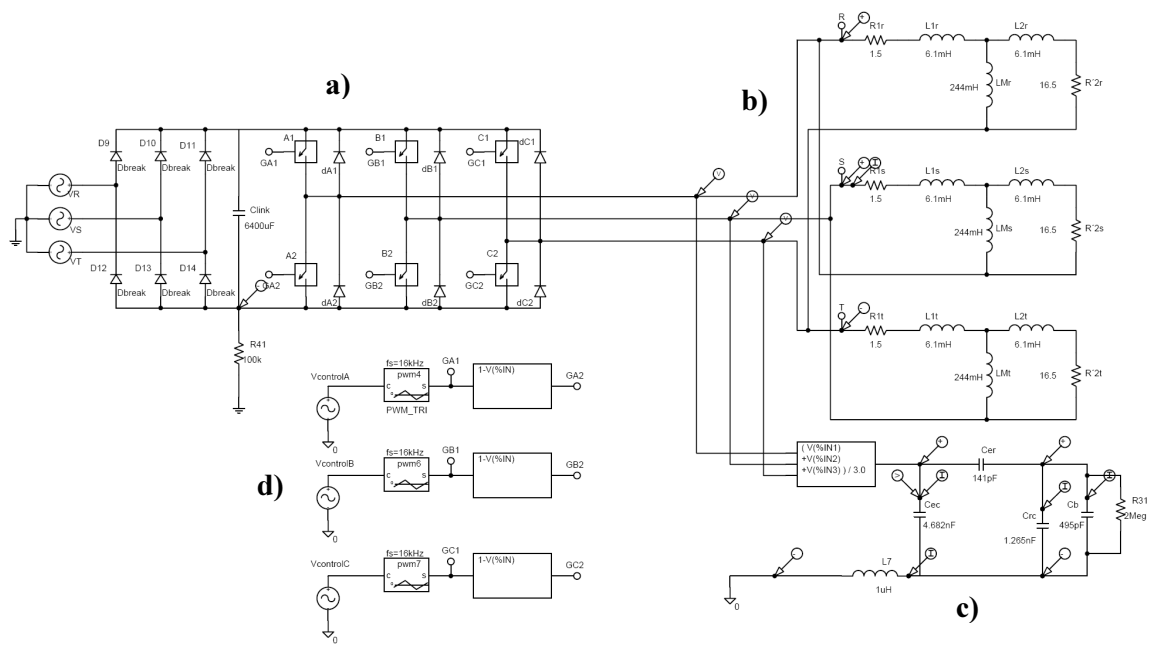
Figure 23. Schematic circuit used for simulation in Pspice [40]

Figures 24 and 25 show the waveforms of various quantities of interest for the three-phase induction motor 1Hp IM1hp1, Figures 26 and 27 show the waveforms for the three-phase induction motor of 1 Hp IM1hp2.
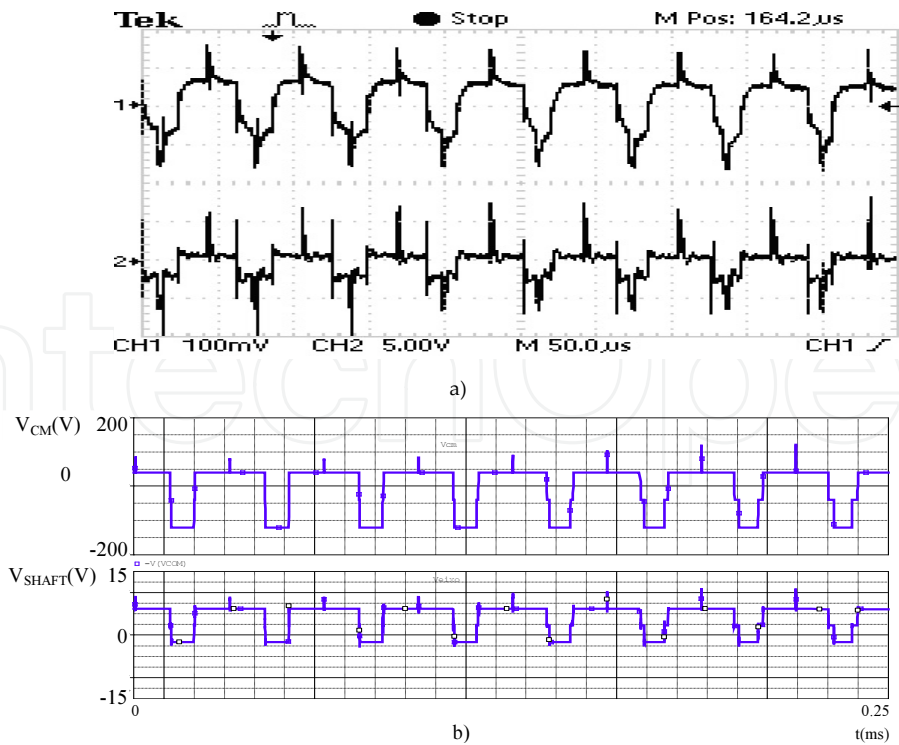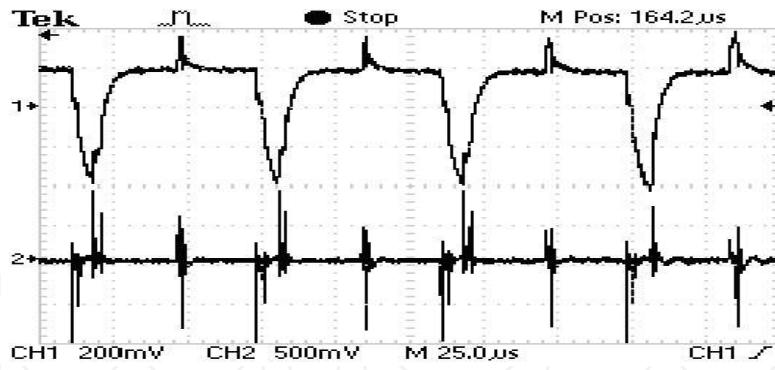

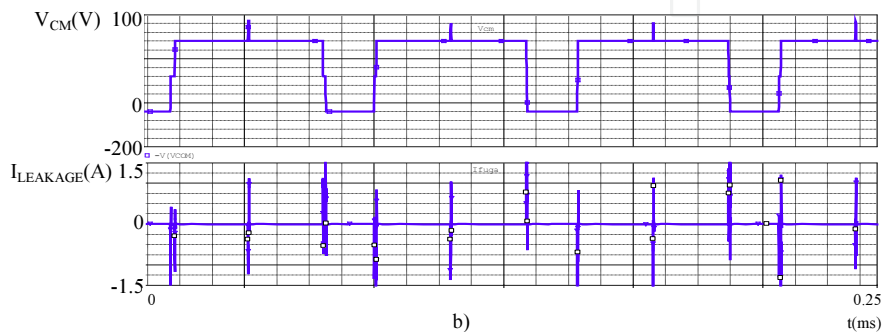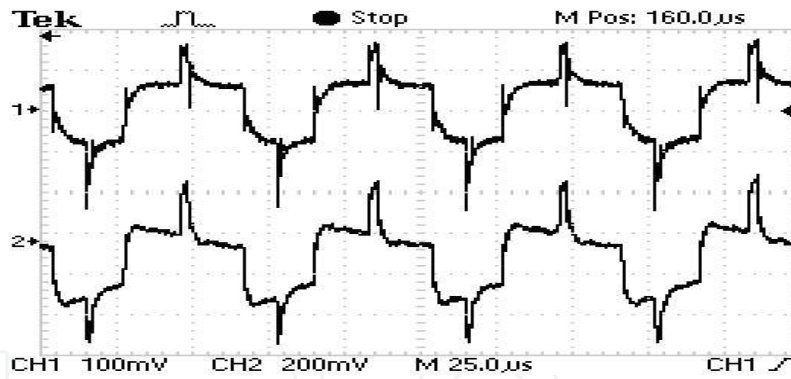**Figure 24.** V_{CM} – CH1, V_{SHAFT} – CH2; a) measured, b) simulated (IM1hp1)
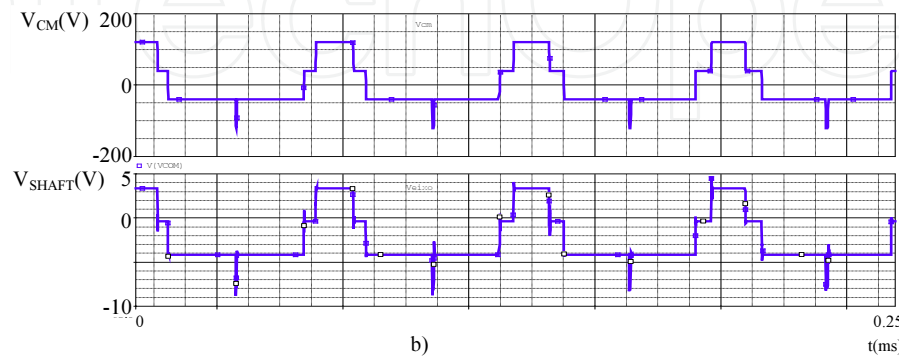
Figure 25. V_{CM} – CH1, $I_{LEAKAGE}$ – CH2; a) measured, b) simulated – (IM1hp1)

Figure 26. V_{CM} – CH1, V_{SHAFT} – CH2 - a) measured, b) simulated - (IM1hp2)
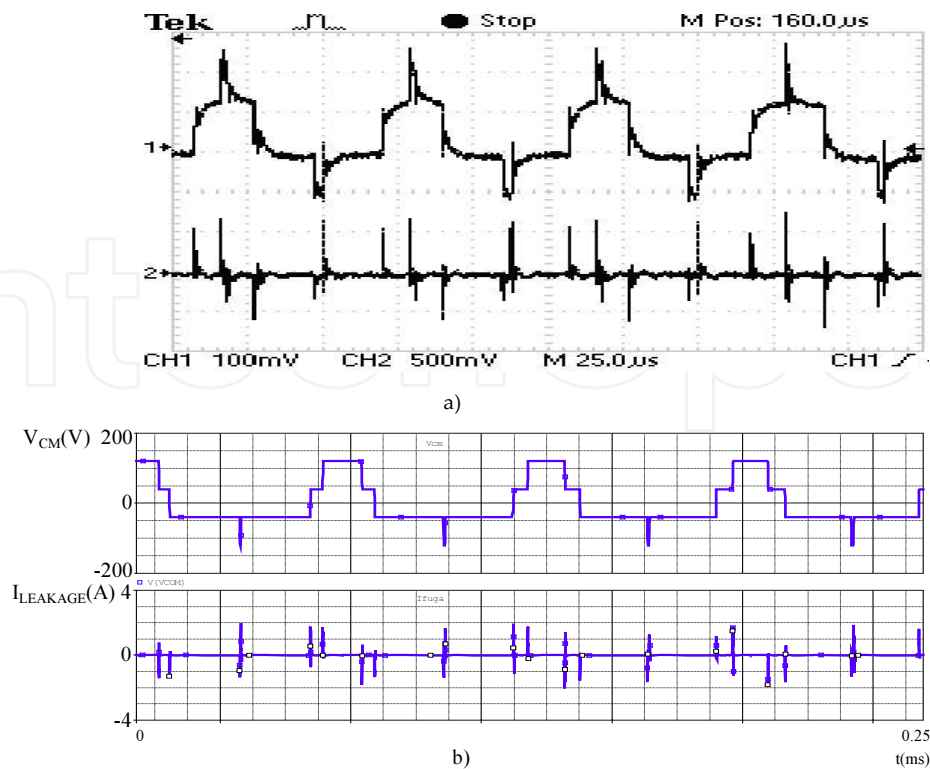
Figure 27. V_{CM} – CH 1, $I_{LEAKAGE}$ – CH 2 - a) measured, b) simulated - (IM1hp2)

5. Results and conclusions

In the comparison of results between the two 1Hp motors (IM1hp1 and IM1hp2), the following considerations are made: (a) Although the motors are of the same power and the same manufacturer, one of them underwent maintenance and the other still has its original compo-nents. This results in differences in the values of capacitances C_{SF}, C_{RF}, and C_B. The exchange of maintaining consisted of stator conductors, insulating layer placed in the stator slots, and replacing the original bearings. These changes result in different values of capacitances, although they present very similar values. (b) The use of sensors of both voltage and current characteristics more suitable for this type of experiment such as precision operation range, frequency response, are necessary to avoid problems like those that occurred mainly in the measurements of the motors on the switching frequency of 4 kHz [40]. (c) There was no automation of measurements of quantities of interest according to the equipment available for this purpose. Thus, measurement errors were the same, but it can still be said that they were within a satisfactory tolerance, when comparing these two motors. In Table 8, comparisons are shown between the parasitic capacitances for two 1Hp motors.

The methodology for determining the parasitic capacitance of the induction motor, when driven by a PWM inverter presents consistent and coherent results.

The results of the tests have revealed that the parasitic capacitances of the induction motor are a function only of the geometric-constructive characteristics [40, 41].

Inverter Switching Frequency (kHz)	Motor Frequency (Hz)	C_{SF} (pF)	C_{RF} (pF)	C_{SR} (pF)	C_B (pF)
16					
Motor	20	1997,33	1199,87	60,53	283,61
1Hp	30	1991,15	1194,67	61,00	226,18
IM1hp1	40	1982,45	1189,56	60,87	216,28
	50	1959,52	1187,41	61,01	207,91
	60	2014,87	1203,23	62,72	185,64
16					
Motor	20	2036,24	1212,65	58,06	749,66
1Hp	30	2107,39	1196,70	58,72	554,36
IM1hp2	40	2104,88	1212,93	60,35	349,10
	50	2027,39	1215,36	59,69	196,66
	60	2163,08	1280,51	64,68	172,38

Table 8. Comparison between the parasitic capacitances of 1Hp motors

The switching frequency variations almost do not change the values of the capacitances. In fact, the quantity which have their values changed due the variation of switching frequencies is the reactance of these capacitances. High switching frequency of the PWM inverter, despite improving the characteristic shape of the load current wave, causes the switching time of power electronic devices (IGBT or MOSFET) to be rather low, resulting in increased rates of growth of voltage (dV/dt) [7]. This reflects directly on the currents flowing through the parasitic capacitances and therefore the leakage current.

Also there is an increase of the amplitude of these currents due to the capacitive reactance parasites being substantially diminished in value due to the increase of the switching frequency. So, the effects of electromagnetic interference are increased both on bearings (bearing currents) as on capacitive currents in the motor. It is also noticed that the bearing of capacitance values (C_B) decrease with increasing induction motor speed [10].

Common mode filters are used to minimize the effects of currents flowing through the parasitic capacitances of the induction motor. The accurate determination of these capacitances values, using the methodology proposed in this section, has the main objective of optimizing the design of these filters.

This optimization implies a more accurate and reliable specification of the components used in filter design, thus providing a significant reduction of volume and weight of the filter; the number of components used, and thus cost reduction thereof.

Author details

Rudolf Ribeiro Riehl[1*], Fernando de Souza Campos[1], Alceu Ferreira Alves[1] and Ernesto Ruppert Filho[2]

*Address all correspondence to: rrriehl@feb.unesp.br

1 São Paulo State University, Unesp, Bauru, Brazil

2 State University of Campinas, Unicamp, Campinas, Brazil

References

[1] Busse, D., Erdman, J., Kerkman, R. J., Schlegel, D., and Skibinski, G. System Electrical Parameters and Their Effects on Bearing Currents, *IEEE Trans Indus Applicat*, Vol. 33, no. 2, pp. 577-584, 1997.

[2] Erdman, J., Kerkman, R. J., Schlegel, D., and Skibinski, G. Effect of PWM Inverters on AC Motor Bearing Currents and Shaft Voltages, *IEEE APEC Conf*, Vol. 01, pp. 24-33, 1995.

[3] Akagi, H., Hasegawa, H., and Domouto, T. Design and Performance of a Passive EMI Filter for Use with a Voltage-Source PWM Inverter having Sinusoidal Output Voltage and Zero Common-Mode Voltage, *IEEE Trans Power Electron*, Vol. 19, no. 4, pp. 1069-1076, 2004.

[4] Busse, D., Erdman, J., Kerkman, R. J., Schlegel, D., and Skibinski, G. Bearing Currents and their Relationship to PWM Drives, *IEEE Trans Power Electron*, Vol. 12, no. 2, pp. 243-252, 1997.

[5] Villabona, E. G., Gúrpide, P. S., Sádaba, O. A., Azanza, A. L., and Palomo, L. M. Simplified High-Frequency Model for AC Drives, *IEEE Conf Indus Electron Soc*, Vol. 02, pp. 1144-1149, 2002.

[6] Naik R., Nondahl, T. A. Nondahl, Melfi M. J., Wang, and J. S. Wang. Circuit Model for iShaft Voltage Prediction in Induction Motors Fed by PWM-Based AC Drives, *IEEE Trans Indus Applic*, Vol. 39, no. 5, pp. 1294-1299, 2003.

[7] Charoy, A. and Dunand, P. Bearing Current Induced by a Power Drive, *Automot Power Electronics*, pp. 01-07, Paris, 2007.

[8] Boglietti A., Cavagnino A., and Lazzari M. Experimental High Frequency Parameter Identification of AC Electrical Motors, *IEEE Trans Indus Applic*, Vol. 43, no. 01, pp. 23-29, 2007.

[9] Akagi H. and Doumot T. An Approach to Eliminating High-Frequency Shaft Voltage and Ground Leakage Current from an Inverter-Driven Motor, *IEEE Trans Indus Applic*, Vol. 40, no. 4, pp. 1162-1169, 2004.

[10] Akagi, H. and Tamura, S. A Passive EMI Filter for Eliminating Both Bearing Current and Ground Leakage Current from an Inverter-Driven Motor, *IEEE Trans Power Electron*, Vol. 21, no. 5, pp. 1459-1469, 2006.

[11] Kempski, A. Capacitively Coupled Discharging Currents in Bearings of Induction Motor Fed from PWM (pulsewidth modulation) Inverters, *J Electrostatics*, vol. 51-52, pp. 416-423, 2001.

[12] Adabi, J., Zare, F., Ledwich G., and Ghosh, A. Leakage Current and Common Mode Voltage Issues in Modern AC Drive Systems, *Australasian Universities Power Engineering Conference, 2007 (AUPEC 2007)*, pp. 01-06, 2007.

[13] Muetze, A. and Binder, A. Calculation of Motor Capacitances for Prediction of Discharge Bearing Currents in Machines of Inverter-Based Drive Systems, *IEEE International Conference on Electrical Machines and Drives*, pp. 264-270, 2005.

[14] Chen, L., Lipo, T. A., and Fitzgerald, D. Measurement and Analysis of Induction Motor Bearing Currents in PWM Inverter Drives, *IEEE Trans Indus Applic*, Vol. 32, pp. 1365-1370, 1995.

[15] Esmaeli A., Jiang B., and Sun, L. Modeling and Suppression of PWM Inverter's Adverse Effects, *1st International Symposium on Systems and Control in Aerospace and Astronautics*, EI&IEEE, pp. 1450-1454, China, 2006.

[16] Arnedo, L. and Venkatesan, K. Pspice Simulation for Conducted EMI and Overvoltage Investigations in a PWM Induction Motor Drive System, *IEEE Workshop on Computers in Power Electronics*, pp. 132-137, 2002.

[17] Boglietti, A. and Carpaneto, E. An Accurate High Frequency Model of AC PWM Drive Systems for EMC Analysis, *IEEE Indus Applic Conf*, Vol. 2, pp. 1111-1117, 2001.

[18] Melly, S. New Output Filter Concept for Power Drive Systems, *Product Marketing*, SCHAFFNER, pp. 01-08, 2002.

[19] Lai, Jih-Sheng, Xundong, H., Pepa, H., Chen, S., and Nehl, T. W. Inverter EMI Modeling and Simulation Methodologies, *IEEE Trans Indust Electron*, Vol. 53, no. 3, pp. 736-744, 2006.

[20] Chen, S., Lipo, T. A., and Fitzgerald, D. Source of Induction Motor Bearing Currents Caused by PWM Inverters, *IEEE Trans Energy Conver*, Vol. 11, no. 1, pp. 25-32, 2006.

[21] Bogel, B., Christiansen, T., Friis, C., Pedersen, N., and Valsson, T. Active EMI Filter for Common Mode Noise Suppression in Three-Phase Drives, PED2001, 2001.

[22] Muttaqi, K. M. and Haque, M. E. Electromagnetic Interference Generated from Fast Switching Power Electronic Devices, *Int J Innovat Energy Sys Power*, Vol. 3, no. 1, pp. 19-26, 2008.

[23] Kerszenbaum, I. Shaft Currents in Electric Machines Fed by Solid-State Drives, *IEEE Industrial and Commercial Power Systems Technical Conference*, pp. 71-79, 1992.

[24] Ramachandran, A., Reddy, M. C., and Moodithaya, R. Minimization and Identification of Conducted Emission Bearing Current in Variable Speed Induction Motor Drives Using PWM Inverter, *Sādhanā*, Vol. 33, no. 5, pp. 615-628, 2008.

[25] Mäki-Otto, P. *Modeling and Reduction of Shaft Voltages in AC Motors Fed by Frequency Converters*, Doctoral Dissertation, Helsinki University of Technology, 2006.

[26] Boldea, I. and Nasar, S. A. *The Induction Machine Handbook*, CRC Press, New York, USA, 2002.

[27] Fitzgerald, A. E., Kingsley, C., and Umans, S. D. *Electric Machinery*, McGraw-Hill, 6th Edition, New York, USA, 2003.

[28] Mohan, N., Undeland, T. M., and Robbins, W. P. *Power Electronics – Converters, Applications and Design*, John Wiley & Sons Inc., USA, 2003.

[29] Movidrive MDX60B/61B Catalog, SEW Eurodrive, 2005.

[30] Rashid, M. H. *Spice for Power Electronics and Electric Power*, Prentice-Hall, NJ, USA, 1993.

[31] MOVTOOLS Software – Motion Studio V.5.60, SEW-Eurodrive, 2009.

[32] Paton, B. LABVIEW – Fundamentals of Digital Electronics, National Instruments Corporations, USA, 1998.

[33] Get Starting with LabVIEW, National Instruments Corporations, USA, 2007.

[34] LabVIEW Fundamentals, National Instruments Corporations, USA, 2007.

[35] LabVIEW 8.5 Software, LabVIEW Profissional Development System, National Instruments Corporations, USA, 2007.

[36] PSPICE Schematics 9.2 Software, Cadence Design Systems, USA, 2000.

[37] Ribeiro Riehl, R. and Ruppert, E. High Frequency Parameters of Small Three-Phase Induction Motors for Operation with PWM Inverters. *Int Electric Mach Drives Conf – IEMDC*, Vol. 01, pp. 1352-1357, Miami, USA, 2009.

[38] Ribeiro Riehl, R. and Ruppert, E. A Simplified Method for Determining the High Frequency Induction Motor Equivalent Electrical Circuit Parameters to be used in EMI Effect – ICEMS 2007, pp. 1244-1248, Seoul, Korea, 2007.

[39] Ribeiro Riehl, R. and Ruppert, E. High Frequency Capacitances Determination in Three-Phase PWM Inverter-Motor Drive System Using an Alternative Method Applied to EMI Effect Studies. 9º. Congresso Brasileiro de Eletrônica de Potência – COBEP, vol. 01, pp.137-141, Blumenau, Brazil, 2007.

[40] Ribeiro Riehl, R. and Ruppert, E. *A Methodology to Determine the Parasitic Capacitances of the Squirrel-Cage Three-Phase Induction Motors*, PhD Thesis, FEEC-UNICAMP, Campinas, SP, Brazil, 2010.

[41] Ribeiro Riehl, R. and Ruppert, E. Experimental Method for Determining the Parasitic Capacitances of Three-Phase Induction Motor Driven by PWM Inverter. *Sba Controle & Automação* [online]. 2012, Vol. 23, no. 2, pp. 153-163. ISSN 0103-1759

[42] Ribeiro Riehl, R., Covolan Ulson, J.A., Andreoli, A.L., and Ferreira Alves, A. A Simplified Approach for Identification of Parasitic Capacitances in Three-Phase Induction Motor Driven by PWM Inverter, *Electrical Machines and Systems (ICEMS), 2014, 17th International Conference on*, Vol., no., pp. 2550,2554, 22-25 Oct. 2014.

[43] Romanenko, A., Ahola, J., Muetze, A., and Niskanen, V. Study of Incipient Bearing Damage Monitoring in Variable-Speed Drive Systems, *Power Electronics and Applications (EPE'14-ECCE Europe), 2014 16th European Conference on*, Vol., no., pp. 1,10, 26-28 Aug. 2014.

[44] Tallam, R.M., Valdez, C.D.R., Kerkman, R.J., Skibinski, G.L., and Lukaszewski, R.A. Common-Mode Voltage Reduction for Regenerative AC Drives, *Energy Conversion Congress and Exposition (ECCE), 2012 IEEE*, Vol., no., pp. 3301,3308, 15-20 Sept. 2012.